Chapter 3

JUST ADD (DEUTERATED) WATER:

PASSIVE TRACER AND MINIMAL CARBON AND NITROGEN AMENDED SIP-NANOSIMS INCUBATIONS PROVIDE AUTHENTIC ESTIMATES OF DEEP BIOSPHERE ACTIVITY IN 2,000 MBSF COALBEDS

Abstract

The past decade of marine scientific drilling has led to the discovery of seemingly ubiquitous microbial life in a range of deep biosphere habitats. In a quest for possible depth limits to deep life, IODP Expedition 337 successfully recovered core down to a record-breaking 2.5 km below seafloor from a deeply buried coalbed system with low thermal alteration. Isotopic signatures and taxonomic profiles suggested a typical a microbial assemblage, partnering fermentive bacteria and methanogenic archaea, which degrades coal into end products of methane, carbon dioxide, and hydrogen. The previously established global depth trend for subseafloor microbial abundance suggests ~ 10^5 cells/cm^3 at 2 kmbsf, instead cell abundances were 10 cells/cm^3 or less in most samples below 1.5 km suggesting life-limiting conditions may have been reached. The coalbeds, however, were comparative "hot spots" with cell concentrations 10 to 100 × higher than surrounding lithologies. Methy-compounds derived from coal decomposition may serve as potential carbon sources for this coalbed microbial community. To determine general microbial activity and methyl-compound utilization, 2.5 year-long Stable Isotope Probing (SIP) incubations were carried out at in situ temperatures (45 ^{o}C) with deuterated water (passive tracer) and minimal ^{13}C-carbon and ^{15}N-nitrogen amendments. Incubation geochemistry was non-destructively monitored during incubation to track activity, with NanoSIMS analysis performed on the most methane-producing incubations at the end of the incubation period. While cells were scarce, ranging from 50 to 2000 cells/cm^3 in the most active incubations, we estimated average hydrogen and nitrogen biosynthesis-based turnover times of less than a year to 63 years and less than a year to 2,020 years, respectively. NanoSIMS carbon biosynthesis-based turnover time estimates were orders of magnitude lower than previous deep biosphere studies, but bulk catabolic were rates similar to shallower hydrocarbon seep sediments. Our results support the concept of a deep biosphere community focused predominantly on maintenance over growth, but with much faster turnover times than previous estimates.

Introduction

Advances in deep sea drilling technology and microbiological methods have led to the discovery of microbial life in a range of deep biosphere habitats, from Earth's most oligotrophic sediments (IODP Expedition 329) to its largest aquifer (IODP Expedition 336). While approximations of total deep life cell abundance continue to evolve, currently estimated to be ~ 10^{29} cells in marine sediments (Parkes et al. 2014), the deep biosphere undoubtedly constitutes a massive percentage of life on Earth. With their continued detection on missions extending into older, deeper, and hotter habitats over the past decade of deep sea drilling, deep life has been surprisingly ubiquitous given their limited resources. While we have yet to determine what parameters limit deep biosphere cells, they are still less abundant and metabolize more slowly than cultured or surface microbes (Hoehler & Jorgensen 2013). Given that generation times are slower, and opportunities for microbe-microbe interaction are fewer, in the deep marine subsurface (low cell density, lack of fluid flow, expense of flagellar mobility, etc.), it is expected that genetic adaptation and horizontal gene transfer rates are minimal (Hoehler & Jorgensen 2013). It is therefore more likely that persistence in deep biosphere environments is achieved with pre-existing capacity, rather than cells undergoing a period of genetic evolution and adaptation (Biddle et al. 2011; Jørgensen & Marshall 2016). Though as we further constrain biosynthesis rate-based turnover times and cell distribution in the deep biosphere, these genetic evolution assumptions may require revision.

Deep biosphere cell abundance has been described by a global depth trend (log cells/cm^3 = 8.05 - 0.68 log depth (m); Parkes et al. 2014) that predicts a three order of magnitude drop from sediment surface (10^9) to 1 km below seafloor (bsf) (10^6). This trend likely describes factors that co-vary with depth, such as organic carbon availability (Lipp et al. 2008). Similarly connected to substrate availability, cell abundance can also be spatially correlated to distance from land and sedimentation rate (Kallmeyer et al. 2012). However, it is not known how cell enumeration relates to cell activity, of import for understanding the ability of deep life to recycle fossil organic carbon back to the surface biosphere. Subseafloor cell activity is often traced geochemically through the utilization of substrates, such as sulfate, per cell per unit time. Activity can be further parsed into catabolic rates (energy-generating substrate use) and anabolic

rates (biomass-generating substrate use). It is assumed substrate utilization will be diverted more toward energy generation to maintain cell viability than biomass generation since substrates are more limiting at depth. Carbon catabolic rates computed from sulfate reduction coupled to acetate oxidation at 1.5 mbsf are ~ 10^{-4} fmol C/cell/day when measured by ^{35}Sulfate incubation for Peru Margin sediments (Parkes et al. 1990) and ~ 10^{-6} fmol C/cell/day when measured by porewater fluxes for Pacific Gyre sediments (D'Hondt et al. 2002). These rates can be compared to ~ 10^{-2} fmol C/cell/day measured in shallow marine sediments of Aarhaus Bay by the same method (Leloup et al. 2009). From the radio-labeled sulfate reduction technique, it appears catabolic rates decrease with depth, but absolute rate estimates vary depending on study location.

Anabolic rates have been estimated by multiple means and are often converted to turnover times for a given element in biomass (H, C, or N). Bulk sediment D:L amino acid racemization modeling in eastern tropical Pacific sediments (~ 200 mbsf) resulted in degradation-based turnover times of 2,000-3,000 years, with total organic carbon turnover estimated at 43 million years (Lomstein et al. 2012). Estimates from biosynthesis based-turnover of microbial lipids have a similar lower estimate (1,600 years), but a much higher upper estimate (73,000 years; Xie et al. 2013). Natural abundance carbon single-cell-Secondary ion mass spectrometry (SIMS) combined with diagenetic models and a pure culture (*Acetobacterium*) slow metabolism proxy for required cellular maintenance energy, yield carbon degradation rate-based turnover times of 70 to 2,150 years (Biddle et al. 2006). Single-cell NanoSIMS carbon and nitrogen biosynthesis rates from (stable isotope probing) SIP incubations with Shimokita Peninsula sediments (219 mbsf) determined much faster turnover times, from 63 to 192 days (Morono et al. 2011). In these experiments, ^{13}C-glucose addition had the highest number of carbon incorporating cells (76%), suggesting most cells were viable when high-energy substrates were provided. Since these NanoSIMS single-cell anabolic rates were based on conditions with higher substrate concentrations than would have been accessible to the in situ microbial community, these results may inform viability more than in situ rates of metabolism.

To probe the depth limit of life, IODP Expedition 337 sampled a deeply buried (~ 2 kmbsf) coalbed system of terrestrial origin and low thermal alteration (~ 25 mya lignite to sub-bituminous, as described in Gross et al. 2015). In addition to increased depth (previous record

1.9 kmbsf; Ciobanu et al. 2014), this site is warmer, has more fossil organic carbon, and stands in contrast to previous marine drilling operations that have focused more on electron acceptor availability (D'Hondt et al. 2015; D'Hondt et al. 2004). It has been hypothesized that the slow temperature rise with burial, and concurrent thermogenic and biotic breakdown of recalcitrant organic matter, may provide a continued biomaterial source for deep life (Fry et al. 2009; Horsfield et al. 2006). The increased temperature may also reduce activation energy barriers, allowing reactions that may not have yielded energy at the sediment surface to become exergonic (Parkes et al. 2007). It is possible that microbial life has been living off this organic carbon since burial, since Shimokita coal has never been subjected to extended thermal alteration through its geologic history (< 60^{o}C; Gross et al. 2015; Inagaki et al. 2015; Konyukhov 2010). The temperatures (~ 45^{o}C) and pressures (~30 MPa) of the 2 km coalbed are also well within known limits of life for piezo-thermophilic life (120 MPa and 108oC; Zeng et al. 2009), but other parameters such as porosity or water availability may still be limiting. A study of the effect pore size has on cell habitability and mobility found particle diameters smaller than 2 μm create trapped cells, and the combined effects of particle size and pressure should render cells dead at 1 kmbsf (Rebata-Landa & Santamarina 2006).

Initial results from Expedition 337 showed cell abundances no longer tracked the global depth trend (log cells/cm^3 = 8.05 - 0.68 log depth (m); Parkes et al. 2014), suggesting that life-limiting conditions had been reached (Inagaki et al 2015). The coalbed, however, was a comparative "hot spot" for microbes with 10 to 1000 times higher cell concentrations than the adjacent shale and sandstone environments (≤ 10 cells/cm^3; Inagaki et al. 2015). Though even the coalbed cell abundances were much lower than the global depth trend estimate of ~ 5.5 × 10^5 cells/cm^3 for 2 kmbsf. Based on geochemistry, carbon and hydrogen should not be limiting at this depth. Since temperature, pressure, and substrate availability are well within life limits, pore space and/or water availability may be the limiting factors. Despite these low cell concentrations, geochemical and genomic data suggest an active microbial coalbed assemblage was not only present, but phylogenetically resembled the microbial community of its paleo-surface expression (terrestrial swamp; Inagaki et al. 2015). While no archaeal 16S rRNA genes were recovered with Illumina Tag (iTag) sequencing, geochemical and biomarker analyses supported the existence of an active methanogenic community, as well. Since recovered cells appear to be

from an indigenous community rather than later colonization of allochthonus microbes, the microbial community profile supports the idea of a microbial bioreactor buried and sustained for millions of years post deposition.

Many questions remain as to how these still active, coalbed cells are compared to other deep biosphere and surface environments. How is activity is distributed across the viable microbial assemblage? How is activity split between anabolic and catabolic modes? How are resources split between carbon and nitrogen acquisition? Answering these questions requires single-cell techniques to address sub-population dynamics and is most informative if the natural system is minimally perturbed. Measuring activity in the deep biosphere requires a balance between stimulating the population enough to observe a metabolic signal and over-stimulation of the system such that experimental concentrations no longer approximate in situ conditions, or are even detrimental (Postgate & Hunter 1963).

D_2O is a passive (non-nutrient), universal tracer with an extremely low natural abundance (0.015 %) for high detection rates. These combined factors are ideal for activity detection in slow growing, low biomass systems where the metabolic diversity may not be known a priori, such as the deep biosphere. D_2O utility can be extended by use in conjunction with other isotopically labeled or unlabeled substrates to characterize substrate specific activity along with basal anabolic rates for mixed-community, environmental samples. Utilization of D_2O as a passive tracer of anabolic activity has been successfully applied in pure culture and mammalian microbiome studies (Berry et al. 2015; Kopf et al. 2015; Kopf et al. 2016), soils (Eichorst et al. 2015), and methane-rich environments (Kellermann et al. 2016; Wegener et al. 2012). This technique can provide single-cell biosynthesis rates when used in conjunction with NanoSIMS (Kopf et al. 2015). D_2O incorporation can also be measured by other single-cell techniques such as Raman scattering (Berry et al. 2015), but this method requires much higher labeling for detection and is therefore not ideal for low activity systems.

Here, we conducted long-term (2.5 yr) SIP incubations with a passive tracer (D_2O) and minimal ^{13}C (30 μM C) and ^{15}N (3 μM N) amendments of environmentally relevant substrates to determine the in situ activity of microorganisms associated with a paleo-terrestrial swamp after

burial for millions of years. Incubations were prepared from six separate cores ranging from 1377 to 2466 mbsf and one blend of five lithologies from 1950 to 2000 mbsf. Two coalbeds were included in these seven incubations, a shallower (~ 1920 mbsf) coal-only sample deposited under more marine-influenced conditions, and a deeper coalbed (~ 2000 mbsf) deposited under more limnic conditions included in the mixed lithology sample. Fifty-two incubation carbon amendment and control conditions interrogating a range of potential deep biosphere metabolic strategies were prepared onboard (Inagaki et al. 2012). Methylamine and methanol, coalbed fermentation and degradation byproducts, and methane, terminal product from utilizing methyl-compounds (Strąpoć et al. 2011), were used as the basis for the methylotrophic subset of incubations returned to Caltech. Of these amendments, methylamine and methanol were the most active based on geochemical monitoring during incubation, and are discussed here. Our SIP incubations amended with methyl substrates, deuterated water, hydrogen and ammonium provide catabolic rates and basal and substrate-specific biosynthesis rates of single cells from the deepest samples ever retrieved by scientific ocean drilling, showing distinct responses in microbial activity and substrate utilization between coalbeds. The reciprocal of these rates also provides estimation of biosynthesis-based turnover times for hydrogen, nitrogen, and carbon that are faster than previous deep biosphere estimates by other methods.

Materials and Methods

Incubation preparation

IODP Expedition 337 operations commenced July 26 and continued through September 30, 2012 on the *D/V Chikyu*. Utilizing riser drilling, we penetrated a sedimentary sequence down to 2466 mbsf. The borehole site is off the Shimokita Peninsula in 1180 m water (Supplemental Figure 1). With depth, the drilled sequence transitions from open marine (youngest; late Pliocene, ~ 5 Ma) to terrestrial (oldest; late Oligocene, ~ 30 Ma) (Figure 1; adapted from Gross et al. 2015). Shipboard sedimentological and geochemical analysis and microbiological methods (including contamination controls) can be found in the Expedition 337 Proceedings volume (Inagaki et al. 2012). Additional coal petrography is available in Gross et al. 2015.

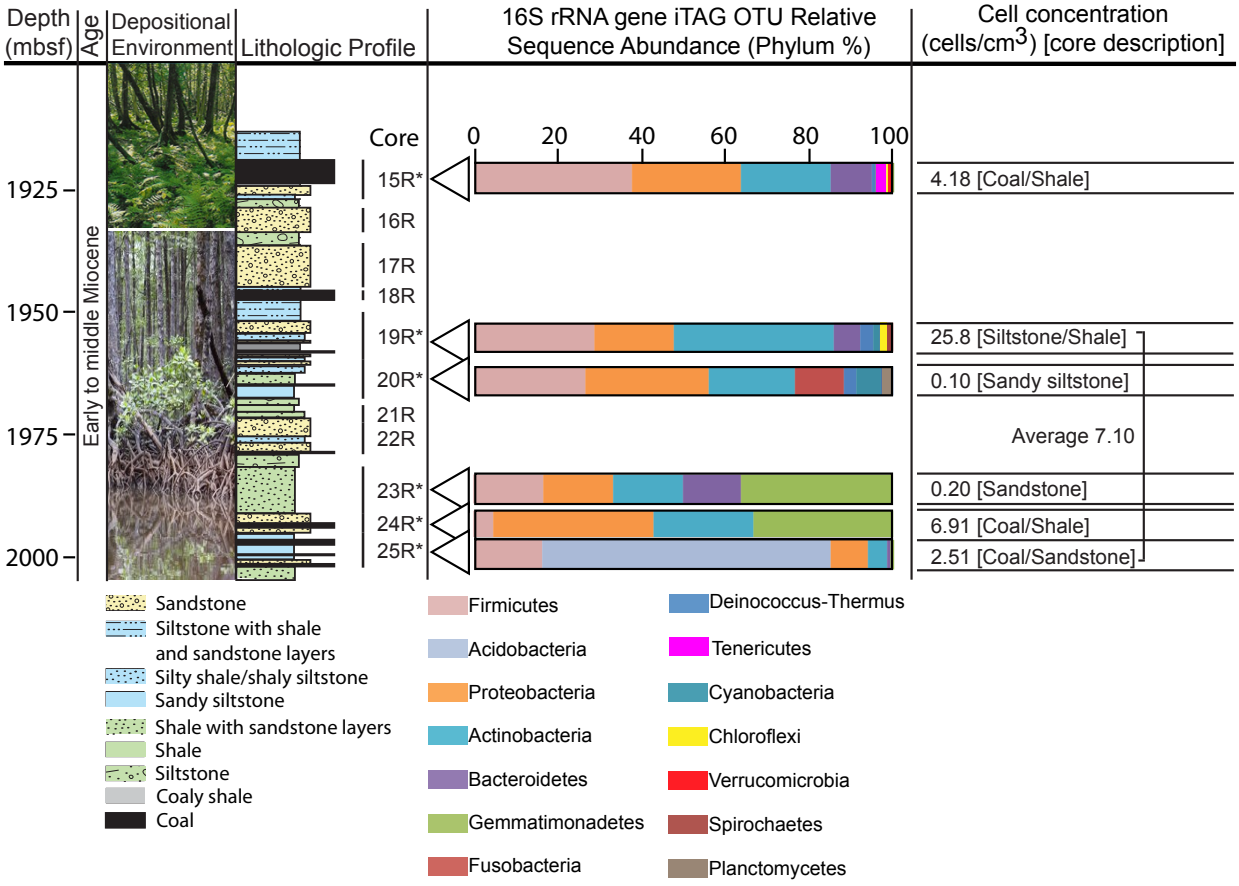

Figure 1: Description of samples collected on IODP Expedition 337 that were incubated for SIP-NanoSIMS. Sample depth, biostratigraphic age, inferred depositional environment, and lithologic profile with location of main coal bearing cores (adapted from Gross et al 2015). *Indicates cores used for SIP NanoSIMS analysis, where 15R was used for coal-only incubations and the remaining cores were combined in mixed lithology samples. 16S rRNA gene iTag relative sequence abundance profile demonstrates phylum level distinctions between lithologies sampled. Cell concentrations are most likely indigenous estimates (Inagaki et al. 2015) with broad core description in brackets.

Two sample types, of the seven prepared onboard, were analyzed by NanoSIMS in this study. The first was a coal-only sample from core 15R (1921 mbsf), termed "15R3 coal" (Figure 1). The second was a homogenized core mixture from multiple horizons (19R1, 19R5, 19R7, 20R3, 23R6, 23R8, 24R3, 25R1, 25R2, and 25R3; spanning 1950-1999 mbsf) containing lower coalbed samples, termed "mixed lithology" (Figure 1; *). All incubated samples are early to middle Miocene. In situ temperatures ranged from 46 to 48 ^{o}C in the sampled region (Supplemental Table 1). Porosity was highest in the sandstone layers and lowest in the coal/shale layers. Formation water sampling yielded pressures between 31 and 32 MPa (~ 300 atm) at the top and bottom of sample cores (Inagaki et al. 2012).

Incubations were prepared as described in the "Single-cell analyses of carbon and nitrogen assimilation rates of subseafloor microbes" section of cruise Methods (Expedition 337 Scientists 2013). Briefly, outer drill-fluid contaminated layers of core samples were removed under nitrogen and the remaining core was manually crushed into cm-sized pieces under sterile, anaerobic conditions and distributed evenly into 50 ml glass vials with butyl rubber stoppers and screw caps (NICHIDENRIKA-GLASS Co. Ltd.). Vials were flushed with argon and pressurized to 1 atm headspace. Minimal C, N, and S-free, 20% D_2O (Cambridge Isotopes) media was prepared anaerobically and 20 ml was added to each vial. 20% D_2O had little to no (depending on organism) observable effect in pure culture evaluations of toxicity (Berry et al. 2015; Kopf et al. 2015). A timepoint 1, timepoint 2 and autoclaved vial were prepared for each substrate condition. Timepoint 1 was incubated for six months. Timepoint 2 and autoclaved samples were incubated for 2.5 years and were used for NanoSIMS analysis.

Amendments and incubation conditions for the methyl-substrate Caltech subset are listed in Table 1. A full list of the incubation conditions prepared onboard are in cruise Methods (Expedition 337 Scientists 2013). All incubations listed in Table 1 were incubated at the cruise-measured coalbed in situ temperature of 45 ^{o}C. Equimolar amounts, 30 μmol C and 3 μmol N, were used across incubation conditions and were provided at 50 at. % (Cambridge Isotopes). $^{13}C/^{15}N$-Methylamine (with and without hydrogen amendment, added as 5 ml overpressure to 30 ml headspace volume) was provided as both a carbon and nitrogen source, which could be used for catabolism (methanogensis) or anabolism. ^{13}C-Methanol was provided as a carbon source for catabolism or anabolism in two conditions, one with ^{15}N-ammonium and hydrogen amendments and the other with only ^{13}C-methanol. Background ammonium was ~ 3 mM (as measured by IC) in all incubations, so the 3 μmol ammonium addition at 50 at. % was effectively diluted to 2.7 at. % by the in situ ammonium concentration.

Sampling

After 17 months of incubation (March 2014), all treatments were non-destructively sampled for geochemical analyses. 3 ml of headspace gas was removed to a vial filled with 0.1 M NaOH for methane analysis. The incubation was shaken to suspend smaller sediment particles before liquid was sampled. The liquid was filtered through a 0.1 μm 13 mm Whatman Polycarbonate

Nuclepore Track-Etched Membrane Filter (110405), aliquoting filtrate for DIC and IC analysis. IC samples were frozen and stored at -20 ^{o}C until analysis.

Dissolved Inorganic Carbon Concentration and Isotopic Analysis

DIC samples were injected into prepared He flushed exetainer vials (Labco Limited, Buckinghamshire, UK) containing 100 µl 40% phosphoric acid. Concentrations and stable carbon isotopes of DIC were measured on a Gasbench II (Thermo Scientific, Bremen, Germany) coupled to a Delta V Plus IRMS (Thermo Scientific), following the methods of Torres et al. (2005). Concentrations of DIC were determined based on comparison of the total peak area (masses 44, 45, 46) of replicate sample injections to a standard curve generated from a laboratory standard of $NaHCO_3$. DIC standards were prepared from a solution of 20 mM sodium bicarbonate at 0, 1, 2, 5, 10, 15, and 20 µmol DIC. A 3-pt correction (Coplen et al. 2006) was then applied using NBS 19, internal laboratory standards, and the average of all of the sodium bicarbonate standards. Accuracy was reported as standard deviation (± 0.5 ‰) of the measured $\delta^{13}C$ from NBS-19 and internal laboratory standards as compared to their published values and EA measurements, respectively. Using the estimated error in the volume measurement and the standard deviation of the peak area for the total carbon of bicarbonate standards, the estimated error was ± 0.009 µmol DIC. Labeled substrate solutions were also evaluated for background DIC contamination that could lead to false detection of organic substrate conversion to DIC. Labeled substrate solution DIC was determined to be insignificant.

Methane Concentration and isotopic analysis

Methane headspace concentrations were measured relative to argon (added to circum-equal partial pressure in all incubations) using a Hewlett Packard 5972 Series Mass Selective Detector and Hewlett Packard 5890 Series II Plus Gas Chromatograph at the Caltech Environmental Analysis Center (Supplemental Figure 2). $\delta^{13}C$-CH_4 was analyzed as per methods in Toki et al. (2014) and D-CH_4 was analyzed as per methods in Kikuchi et al. (2016) at Kochi Institute for Core Sample Research, Japan Agency for Marine-Earth Science and Technology (JAMSTEC), Kochi, Japan.

Ion Chromatograph

Parallel Dionex DX-500 (Sunnyvale, CA, USA) ion chromotagraphy systems (Caltech Environmental Analysis Center) were used to measure cations and anions in the incubation filtrate. The anions chloride, acetate, propionate, butyrate, sulfate, oxalate, fumerate, phosphate, and citrate were resolved using an AS11-HC RFIC Analytical column (4 x 250 mm) with an AG11-HC guard column. The cations sodium, potassium, strontium, magnesium, calcium, ammonium, and methylamine were resolved using a CS16 Analytical column. Analyte peak area relative to chloride peak area was used for between sample comparison, rather than absolute concentrations.

Bulk Carbon and Nitrogen Isotopic Measurements with Elemental Analyzer

Total nitrogen, total carbon, and organic carbon were measured by Elemental Analyzer (EA) from 1 - 4 mg sample. Organic carbon was determined by removal of inorganic carbon, dissolved by acidification with 85% phosphoric acid for 2 hours at 50 °C. All samples were lyophilized and transferred to tin capsules (9 × 5 mm). $\delta^{13}C$ and $\delta^{15}N$ of bulk organic matter and weight percent total organic carbon and N (wt.% TOC and TON) were determined via continuous flow (He; 100 ml/min) on a Costech Instruments Elemental Combustion System model 4010 (EA) by oxidation at 980°C over chromium (III) oxide and silvered cobalt (II, III) oxide, followed by reduction over elemental copper at 650 °C. CO_2 was subsequently passed through a water trap and then a 5 Å molecular sieve GC at 50 °C to separate N_2 from CO_2. CO_2 was diluted with helium in a Conflo IV interface/open split prior to analysis. Fast jump was calibrated and applied to switch between N_2 and CO_2 configurations to measure both in the same run. $\delta^{13}C$ and $\delta^{15}N$ values were measured on a Thermo Scientific Delta V Plus irMS. $\delta^{13}C$ and $\delta^{15}N$ values were corrected for sample size dependency and then normalized to the VPDB scale with a two-point calibration (Coplen et al. 2006). Error was determined by analyzing potassium nitrate (NIST ref no: 8549), sucrose (NIST ref no: 8542), and acetanilide (Costech) in combination with in-house standards (urea, glycine, and Hydrate Ridge sediment). Accuracy for C was monitored across all EA analyses and was determined to be 0.14 ‰ (n = 27) and precision was 0.34 ‰ (n = 27, 1σ). Accuracy for N was monitored across all EA analyses and was determined to be 0.16 ‰ (n = 24) and precision was 0.55 ‰ (n = 24, 1σ).

Isotope mass balance was calculated using Equations 2 and 3, where n is the number of moles, F is the fractional abundance (Equation 1) of the rare isotope, and R is the ratio of ion counts of the rare isotope over ion counts of the more abundant isotope (Hayes 2004). F_{total}, n_{total}, $F_{substrate}$, and $F_{background}$ were known. $n_{substrate}$ was solved for given a range of $F_{background}$ sources. $n_{substrate}$ was then divided by the number of days incubation and the total number of cells (cells/cm^3 × cm^3 rock incubated; ~ 7 cm^3) to calculate per cell rates. $F_{background}$ ranged from EA measurements for coal samples to cruise measurements for methane. Natural abundance, background carbon, and stable isotope standard ratios and fractional abundances used are provided in Supplemental Table 1.

$$Equation\ 1:\ F = \frac{R}{1+R}$$

$$Equation\ 2:\ n_{total} = n_{substrate} + n_{background}$$

$$Equation\ 3:\ n_{total} \times F_{total} = n_{substrate} \times F_{substrate} + n_{background} \times F_{background}$$

Sample preparation for NanoSIMS: preservation, separation, enumeration, and FAC sorting

Cell preservation, separation, enumeration, and sorting were all conducted in the clean booth and clean room facilities at Kochi Institute for Core Sample Research, Japan Agency for Marine-Earth Science and Technology (JAMSTEC), Kochi, Japan. 3 ml of incubation headspace was sampled for methane isotope analysis from all coal samples prior to the termination of the incubation experiment (see Methane analysis methods). Half of the solid and half of the liquid portion of each sample were fixed in one 2% paraformaldehyde (PFA) : 3 × phosphate buffered saline (PBS) aliquot overnight. Samples were then subjected to two washes, incubating in 3 × PBS for 6 hrs and then 2 hrs, after each wash respectively. Samples were centrifuged (3500 × g) and supernatant was decanted after each wash. The other half of the sample was preserved in glyTE (70% glycerol, 100mM Tris, 10mM EDTA; Biglow Single Cell Genomics Center preservation protocol) and frozen by cell alive system (CAS) freezing and stored at -80 ^{o}C (Morono et al. 2015).

1 ml rock slurry and ~ 1 g rock chips were subsampled by pipet and sterile cell culture loop, respectively, from the PFA-fixed sample. Cell separation, microscopy, and sorting procedures

followed Morono et al. (2013), with the following modifications: 1) samples were sonicated (Model UH-50, SMT Co. Ltd.) in an ice bath for 20 cycles of 30 sec 200 W, 30 sec off and 2) samples were incubated in hydrofluoric acid post initial sonication, rather than after first density gradient separation. Cell detection limit was 2 cells per entire filter area (diameter 15 mm) as determined by negative controls.

Cells were stained with SYBR Green I (1:40 dilution SYBR Green : TE) and sorted using the cytometry protocol of Morono et al. (2013), with sorted cell collection on indium tin oxide (ITO) coated 0.2 μm polycarbonate filter membranes for direct transfer to NanoSIMS as per Morono et al. (2011) and Inagaki et al. (2015). These filters are termed "NanoSIMS membranes." Indium Tin Oxide (ITO) coatings on polycarbonate membranes (Isopore GTBP02500 Millipore) was developed by sputtering deposition technique at Astellatech Co. Ltd. (Kanagawa, Japan). SEM was imaged with a Zeiss 1550 VP Field Emission Scanning Electron Microscope at the Caltech GPS Division Analytical Facility and SYBR stained cells were imaged with a BX51 epifluorescence microscope (Olympus, Shinjuku, Japan) using 20x (UPlanFL N) dry, 60x (PlanApo N), and 100x (UPlanFL N) oil immersion objectives (Figure 2).

NanoSIMS instrument tuning and analysis

Cell targets were identified (by SYBR stain) and marked on NanoSIMS membranes with a laser dissection microscope (LMD6000; Leica Microsystems) for ease of rediscovery on the NanoSIMS. Samples were analyzed by raster ion imaging with a CAMECA NanoSIMS 50L at the Caltech Microanalysis Center in the Division of Geological and Planetary Sciences. A focused primary Cs^+ beam of ~ 1 pA was used for sample collection, with rasters of 256 × 256 or 512 × 512 pixels. ^{1}H (EM#1), ^{2}H (EM#2), $^{12}C_2$ (EM#3), $^{13}C^{12}C$ (EM#4), $^{12}C^{14}N$ (EM#5), and $^{12}C^{15}N$ (EM#6) were measured simultaneously (see Kopf et al. 2015 for technical development). Collection began after a pre-sputtering of equal intensity to one collection frame (~ 45 min). Recorded images and data were processed using Look@NanoSIMS software (Polerecky et al. 2012). Images were deadtime corrected and individual ion image frames were merged and aligned using the $^{12}C^{14}N$ ion image to correct for drift during acquisition. Single-cell based regions of interest (ROIs) were determined by "interactive thresholding" with the $^{12}C^{14}N$ ion image. Final ion images and counts per ROI were calculated by summation of ion counts for

each pixel over all scans, as shown in Figure 3. Outputs for ROI size and length to width ratio were used to compute cell diameters (Supplemental Figure 3).

A background correction was applied to the $^{13}C/^{12}C$ ratios of cells to correct for instrumental isotope fractionation and to address the low levels of ^{13}C enrichment in cells relative to the background carbon of the ITO coated polycarbonate membrane. In each NanoSIMS frame, an elliptical ROI was drawn in a region with no cells or particles to establish the background $^{13}C/^{12}C$ ratio. A two-point correction was applied to cells using NanoSIMS measurements of the ITO membrane and *Clostridia* spores, both of which were independently measured by EA-IRMS (filter: ^{13}R=0.01067; spores: ^{13}R = 0.01099; see Elemental Analyzer methods). A filter-only correction (no spores) was used for nitrogen, but was not necessary for deuterium because higher signal to background ratio. We also confirmed that cell ROIs had a total C to total N ratio that was distinct from the background correction ROIs and the coal C:N to ensure cell ROIs were all measuring biomass targets.

ROIs were then filtered based on the theoretical precision of the mean for the minor ion, which is equal to square root of the ion count and provided as the Poisson error by Look@NanoSIMS. As a conservative estimate, only ROIs where the deuterium ion count was more than 10 times the Poisson error are presented as violin plots in Figure 4. Data manipulation and display as violin plots of the kernel density function was done using "R" (R Core Team 2015) with the "ggplot2" (Wickham 2009), "dplyr" (Wickham & Francois 2015), "gridExtra" (Auguie 2012), and "RColorBrewer" (Neuwirth 2014) packages. The fractional abundance of all ROIs collected is presented in Supplemental Figure 4, for comparison. Violins are trimmed to the range of the data in both figures and scaled to equal width for visibility in Figure 4 and scaled to number of observations per sample in Supplemental Figure 4 to compare distribution of ROIs between samples.

Equations 5 and 6 were used for biosynthesis production rate calculations, where μ is the biosynthesis production rate (encompassing both cell maintenance and generation of new cells), T_{final} is the length of the incubation, F_{label} is the labeling strength, F_{final} is the single-cell

NanoSIMS measurement, and F_{nat} is the natural abundance. To estimate biomass turnover time, we used Equation 7 ($\tau, Equation\ 7$) as per Zilversmit et al. (1943).

$$Equation\ 5:\ {}^{2}\mu = \left(-\ln\left(1 - \frac{\left({}^{2}F_{final} - {}^{2}F_{nat}\right)}{a_w\left({}^{2}F_{label} - {}^{2}F_{nat}\right)}\right)\right)\Big/ T_{final}$$

$$Equation\ 6:\ {}^{15}\mu = \left(-\ln\left(1 - \frac{\left({}^{15}F_{final} - {}^{15}F_{nat}\right)}{\left({}^{15}F_{label} - {}^{15}F_{nat}\right)}\right)\right)\Big/ T_{final}$$

$$Equation\ 7:\quad \tau = \mu^{-1}$$

NanoSIMS ${}^{2}F$ and ${}^{15}F$ values were multiplied by a conversion factor determined for single cell to bulk isotope measurements in Kopf et al. (2015) of 0.67 (^{2}H) and 0.94 (^{15}N). Since the metabolic pathways utilized by cells in these incubations were unknown, and the proportion of water derived hydrogen in lipids is related to metabolism (Zhang et al. 2009), ^{2}F-based turnover times were calculated using Equation 5 from Kopf et al. (2015) and the full range of lipid water assimilation values (a_w; 0.44 to 0.83) from Zhang et al. (2009). Nitrogen turnover rate calculations assumed all nitrogen was derived from the substrate (methylamine or ammonium), therefore the assimilation constant was excluded from Equation 6. To determine per cell rates, we used values of 5.41 × 10^{-15} moles C per cell and 1.43 × 10^{-15} moles N per cell, which were calculated from 86 fg C/cell and 20 fg N/cell, respectively (Whitman et al. 1998).

Results

Cell Enumeration and Microscopy

Final cell concentrations were computed from cell separates of all incubations (Table 1). By comparison with average cell abundance from bulk core analysis (Figure 1), five (of 8) 15R3 coal incubations had cell concentrations above the method detection limit (1 cell/cm^3) and three incubations were above the background cell concentration estimate (4 cells/cm^3). Mixed lithology had two incubations above detection (of 8), and only one incubation was above background cell concentration (7 cells/cm^3). The highest incubation cell concentration was from

15R3 coal amended with methylamine (1921 cells/cm^3). An extrapolation for maximal doublings if growth began at onset of incubation is also provided for incubations where final cell abundance was above bulk core cell abundance (Estimated doubling time; Table 1). Estimates range between 3 and 8 months, out of the 29-month incubation period.

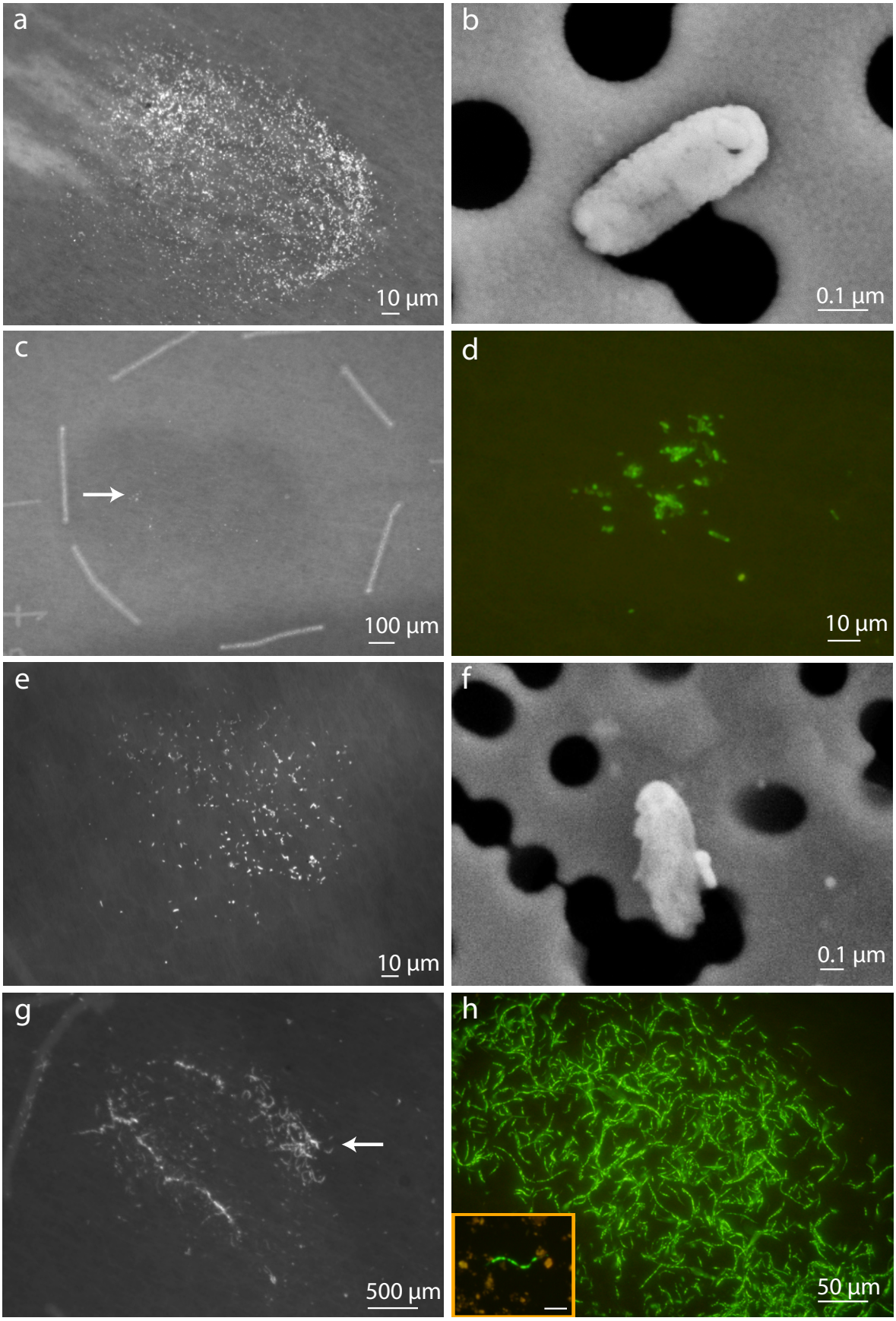
a
10 µm
b
0.1 µm
c
100 µm
d
10 µm
e
10 µm
f
0.1 µm
g
500 µm
h
50 µm

To overcome technical challenges for NanoSIMS analysis of low biomass samples, cell separation and FAC sorting were used to directly concentrate cells in a small analysis area (~ 1 to 0.5 mm^2). This reduces instrument time required to search for microbes by 15-20 times and increased the number of cells per NanoSIMS field of view (0.1 mm^2 out of entire region of 15 mm^2). NanoSIMS membranes (see Methods) were prepared from paraformaldehyde-fixed cell separates of 15R3 coal and mixed lithology samples after 894 days incubation. Examples of concentrated cell separation preparations for the highest cell count samples of 15R3 coal and mixed lithology incubations are provided in Figure 2. When viewed with SYBR staining, most cell morphologies were coccoid (singlets or doublets) or rods (Figure 2 d, e/f), with the exception of incubations that also contained filamentous cells (Figure 2a, b/c). Figure 3c inset is an image of unsorted cell separation, demonstrating how cell sorting both concentrates cells and removes non-target (orange) particles. NanoSIMS cell ROIs were also used to compute cell diameter (length) and length to width ratios (Supplemental Figure 4). Cell lengths fell within the deep biosphere cell size range of 0.2 to 2.1 μm (Kallmeyer et al. 2012), except for the methanol amended mixed lithology incubations that were dominated by filaments. These filamentous cells were also seen in the JAMSTEC collection of mixed lithology incubations with non-methyl substrates (data not shown). Length to width ratios were also within deep biosphere estimates of less than 3:1, with the same filamentous cell exclusion.

Bulk Catabolic Rates

Methane concentration relative to Ar headspace was measured for all coal and mixed lithology samples to determine methanogenic activity (Supplemental Figure 2). While exact concentrations were not determined due to variation between bottles in headspace partial pressures from incubation gas production, 15R3 coal with methylamine had the highest relative

←Figure 2: SYBR stained cells after separation and FACS concentration on ITO coated 0.2 μm polycarbonate NanoSIMS membranes from the two highest cell abundance conditions in 15R3 coal and mixed lithology. SYBR and SEM images highlight some distinctions in cell morphology between the two methanol amended samples. White arrows indicate region of SYBR image on larger membrane target area. a) 15R3 coal amended with methylamine, b) SEM image of a., c) 15R3 coal amended with methanol, d) c. magnified with false color, e) mixed lithology amended with methanol + H_2 + ammonium, f) SEM image of e., g) mixed lithology amended with methanol, and h) mixed lithology amended with methanol magnified with false color (inset is the same sample filtered before cell sorting to demonstrate cell density without concentration, inset bar is 20 μm).

methane concentration of all incubations. Lower, but detectable, levels of methane production were also measured in mixed lithology incubations. Since methane is the expected end product of methylotrophy from the labeled carbon substrates provided, 15R3 coal and mixed lithology were selected for NanoSIMS analysis based on their methane production. Methane ^{13}C and ^{2}H enrichment was also measured for all coal incubations ($\delta^{13}C$-CH_4 and δD-CH_4; Table 1). While incubation methane values (-42.8 to -57.5‰) were enriched in ^{13}C relative to the natural abundance methane values sampled onboard (~ -60 ‰; Inagaki et al., 2015), the minimal ^{13}C enrichment indicated that methane generated in the incubations was primarily derived from sources other than ^{13}C methylated substrates. Incubations were similarly slightly enriched in deuterium (-96.5 to -198.2‰) relative to in situ methane (~ -190 ‰; Inagaki et al., 2015), but unlikely high enough to have been exclusively produced in incubations containing 20% deuterated water.

^{13}C-Methane amended incubation $\delta^{13}C$-DIC ranged from -9 to -3‰. Therefore, enriched ^{13}C-DIC was not seen in any ^{13}C methane incubations that would be expected from active methanotrophy, and these samples were not chosen for further analysis. Methylamine and methanol, however, can be disproportionated to both methane and DIC. Some enrichment in ^{13}C-DIC was observed with methyl-substrates ($\delta^{13}C$-DIC; Table 1), though similar to methane enrichment, ^{13}C-DIC enrichment did not indicate significant DIC was derived from the provided ^{13}C substrate. ^{13}C enrichment above the D_2O-only control condition was higher in methanol-amended conditions than methylamine amended conditions for both 15R3 coal and mixed lithology incubations. DIC concentration was also measured and converted to a per cell production rate (Table 2) for samples with DIC concentration above the D_2O-only condition concentration (0.016 mM DIC 15R3 coal, 0.16 mM mixed lithology). DIC production was 1-3 orders of magnitude higher in mixed lithology than the 15R3 coal samples. Mixed lithology incubations amended with methanol ± hydrogen and ammonium had DIC production of 12 - 0.88 pmol C/cell/day above the mixed D_2O-only condition and were the most enriched in $\delta^{13}C$-DIC of all 15R3 and mixed lithology incubations. 15R3 coal amended with methylamine was the only 15R3 coal sample with DIC production (0.01 ± 0.001 pmol C/cell/day) above the 15R3 coal D_2O-only condition, but it did not produce significant enrichment in the bulk $\delta^{13}C$-DIC pool. While these ^{13}C enrichments would be significant for natural abundance measurements, they are

not significant considering the 50 at. % label used. Since DIC production was not solely from labeled substrates, isotope mass balance calculations were done with a range of potential alternative organic substrates that may also be available in the incubations (methane, -60 ‰; coal derived carbon source, -40 ‰; coal -24 ‰; Supplemental Table 1 for ^{13}R and ^{13}F) that could have been used in conjunction with the labeled substrate to produce the final DIC concentration and isotopic ratios (Table 2). The resulting catabolic rates range from ~ 2.1 to ~ 0.01 fmol C per cell per day for mixed lithology and coal samples, respectively.

Table 1: Incubation lithology, ^{13}C source, ^{15}N source, indication of autoclaved or H_2 added, final cell abundance, extrapolation of maximal days per cell doubling given background and final cell concentrations, and incubation $\delta^{13}C$-DIC (‰), $\delta^{13}C$-CH_4 and δD-CH_4. The cell detection limit was 2 cells per filter area, or ~ 1 cell/cm^3. Errors on DIC measurements are ±0.5 ‰ $\delta^{13}C$-DIC and ±0.0086 µmol DIC. Days incubation at time of DIC measurement was 864 days. *Cell abundances are not from D_2O-only condition but are averaged most likely cell concentration estimates across whole cores from Inagaki et al. (2015) to account for potential heterogeneity between bottles in determining a background cell concentration estimate. MeAm – Methylamine, MeOH – Methanol, Am – Ammonium.

Lith.	^{13}C Source	^{15}N Source	Autocl.	H_2	Abund. (cells cm^{-3})	Est. doubling time (mo.)	$\delta^{13}C$-DIC (‰)	$\delta^{13}C$-CH4 (‰)	δD-CH_4 (‰)
Coal	MeAm	MeAm	Y	Y	BD		-6.0	-42.8	
Coal	MeAm	MeAm	N	Y	4		-3.8	-46.1	-170.4
Coal	MeAm	MeAm	Y	N	BD		-16.2	-57.2	
Coal	MeAm	MeAm	N	N	1921	3.3	-7.2	-55.7	-198.2
Coal	MeOH	Am	Y	Y	BD		19.1	-49.7	
Coal	MeOH	Am	N	Y	2		-6.5	-52.9	-96.5
Coal	MeOH	Am	Y	N	48	8.4	-15.1	-57.5	
Coal	MeOH	Am	N	N	56	7.9	26.7	-56.6	
Coal	*D_2O-only*		*Y*	*N*	*4**		*-10.3*		*-189.0*
Mixed	MeAm	MeAm	Y	Y	BD		5.6		
Mixed	MeAm	MeAm	N	Y	BD		3.3		
Mixed	MeAm	MeAm	Y	N	BD		5.7		
Mixed	MeAm	MeAm	N	N	BD		6.8		
Mixed	MeOH	Am	Y	Y	BD		6.3		
Mixed	MeOH	Am	N	Y	4		14.9		
Mixed	MeOH	Am	Y	N	BD		9.4		
Mixed	MeOH	Am	N	N	129	8.0	44.6		
Mixed	*D_2O-only*		*Y*	*N*	*7**		*4.3*		

Table 2: Isotope mass balance calculations of bulk dissolved inorganic carbon (DIC) production (catabolism) from potential organic carbon sources available in incubations. *Estimated, all other sources from in situ or incubation measurements (Supplemental Table 1). Calculated fmol DIC produced per cell per day with standard deviation (~ 7 cm^3 inoculum per bottle). The error in DIC production is from propagation of μmol DIC measurement.

Lith.	Amendment	DIC prod (pmol C $cell^{-1}$ d^{-1})	σ DIC prod (pmol C $cell^{-1}$ d^{-1})	fmol C/cell/day catabolized from substrate mixed with:		
				Methane	****Coal Derv.***	***Coal***
Coal	MeAm.	0.01	0.001	0.015	0.006	0.005
Mixed	MeOH+H_2+Am.	12.01	0.2			
Mixed	MeOH	0.88	0.01	2.1	1.5	1.3

Single-Cell Anabolic Rates

Representative NanoSIMS ion count (total ^1H, total $^{12}C^{14}N$, and total $^{12}C_2$) and ion ratio ($^2H/^1H$ and $^{15}N/^{14}N$) maps of each incubation showed biomass labeled isotope incorporation in both 15R3 coal (3 out of 8) and mixed lithology (2 out of 8; Figure 3) incubations. Ion ratio maps were not shown for carbon because ^{13}C enrichment above background was not visible. No ^2H or ^{15}N biomass incorporation above background was detected in any autoclaved samples (A), 15R3 coal amended with methanol + ammonium + hydrogen (5 Coal), or mixed lithology amended with methylamine ± hydrogen (1 Mixed and 2 Mixed; Figure 3). Autoclaved 15R3 coal amended with methylamine + hydrogen (1A Coal) and autoclaved mixed lithology amended with methanol (6A Mixed) are provided as examples of NanoSIMS membranes with positive cell identification, but no labeled isotope incorporation, for comparison with active samples. 15R3 coal amended with methylamine (2 Coal) also had evidence of putative germination or cell division (white arrows; Figure 3), where the region of high ^2H and ^{15}N enrichment indicates the daughter cell.

→Figure 3: NanoSIMS analysis of the ^1H, ^{14}N, and $^{12}C_2$ ion counts with $^2H/^1H$ and $^{15}N/^{14}N$ ratio images for 15R3 coal and mixed lithology samples with ^2H and ^{15}N enriched cells. 2 (methylamine) Coal showed evidence for active cell division or germination during the 2.5-year incubation (white arrows), where the parent cell with little ^2H or ^{15}N enrichment is the top arrow and enriched daughter cell is the bottom arrow. Only the daughter cell is evident in the ratio images. Pink arrow provides example of cell that shows no enrichment in the same image. Large ellipses represent background filter correction ROI (see Methods). Two autoclaved samples that have cells with no enrichment are also shown (1A Coal and 6A Mixed). A - autoclaved, Coal – 15R3 coal, Mixed – mixed lithology, 1 - $^{13}C/^{15}N$-methylamine + hydrogen, 2 - $^{13}C/^{15}N$-methylamine, 5 - ^{13}C-methanol + hydrogen +^{15}N-ammonium, 6 – ^{13}C-methanol.

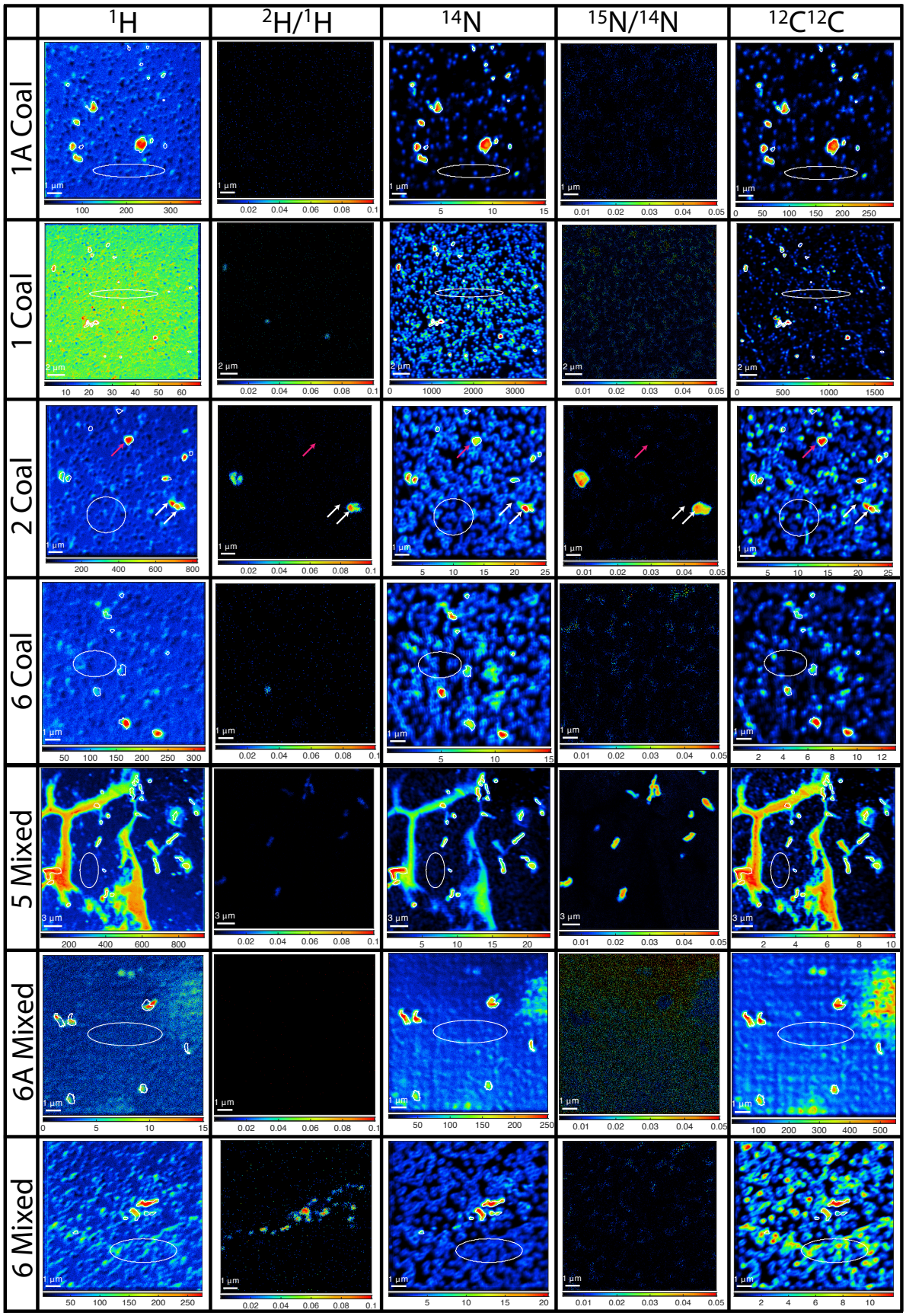
^{1}H
$^{2}H/^{1}H$
^{14}N
$^{15}N/^{14}N$
$^{12}C^{12}C$
1A Coal
1 Coal
2 Coal
6 Coal
5 Mixed
6A Mixed
6 Mixed

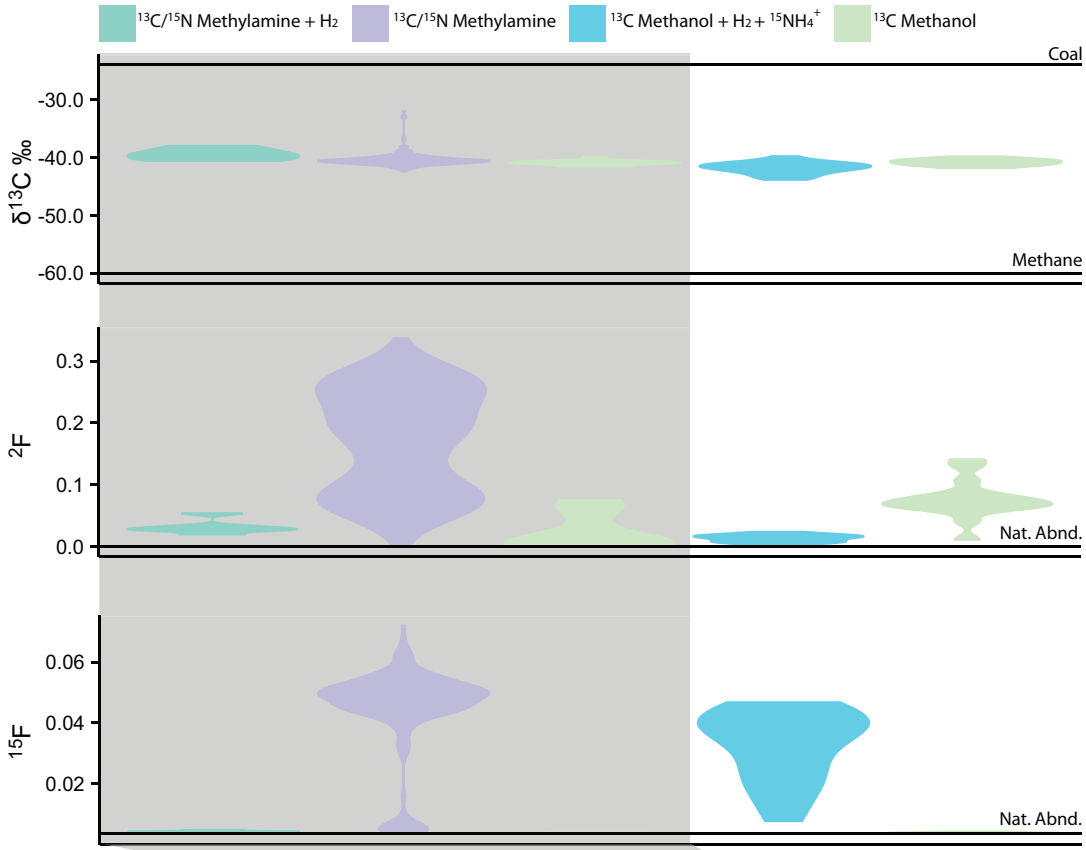

	15R3 Coal			Mixed Lithology	
Number of ROIs	6	176	18	18	15
			Deuterium		
^2F min.	0.01955	0.00222	0.00141	0.00149	0.04199
^2F med.	0.02860	0.18448	0.00651	0.01415	0.07072
^2F max.	0.03332	0.33737	0.07517	0.02387	0.10638
			aw 0.83		
^2F min. Turn. (yr)	20	196	323	302	8
^2F med. Turn. (yr)	13	<1	63	28	4
^2F max. Turn. (yr)	11	<1	4	16	2
			aw 0.44		
^2F min Turn. (yr)	10	103	171	160	4
^2F med. Turn. (yr)	6	<1	33	14	2
^2F max. Turn. (yr)	5	<1	1	8	<1
			Nitrogen		
^{15}F min	0.00405	0.03348	0.00369	0.00738	0.00353
^{15}F median	0.00429	0.04856	0.00377	0.03700	0.00387
^{15}F max	0.00474	0.06280	0.00389	0.04714	0.00429
^{15}F min Turn. (yr)	3408	40	NA	14	NA
^{15}F min Turn. (yr)	2020	26	NA	<1	NA
^{15}F min Turn. (yr)	1153	19	NA	<1	NA
mol N/cell/day	1.15E-21	9.59E-20	NA	2.49E-19	NA
mol N/cell/day	1.94E-21	1.44E-19	NA	2.25E-18	NA
mol N/cell/day	3.39E-21	1.90E-19	NA	2.94E-18	NA

All NanoSIMS cellular ROIs with significant deuterium ion counts (see Methods) are summarized in violin plots (kernel density estimation) of $\delta^{13}C$, ^{2}F, and ^{15}F (Figure 4). Similar to the bulk incubation methane and DIC data, cellular ^{13}C biomass enrichment ranged from -41.85 ‰ to -31.99 ‰ and did not indicate significant labeled substrate assimilation. Using isotope mass balance calculations, we estimated the biosynthesis rate from ^{13}C substrate in conjunction with potential native carbon sources for a range of carbon isotope values that encompass NanoSIMS ROIs (^{13}F 0.01063 to 0.01076; Figure 5). The NanoSIMS values correspond to 0.5 to 4.5×10^{-6} fmol C from substrate per cell per day, i.e. zeptomole range.

While 15R3 coal amended with methylamine did have some cell ROIs (4 out of 233) that were slightly more enriched in ^{13}C, the majority of ROIs for this sample had ^{2}H and ^{15}N biomass enrichment. A total of 212 cellular 15R3 coal amended with methylamine ROIs were defined, 175 of which met the Poisson filter for deuterium ion counts (Figure 4). 99 of the 212 ROIs (47%) have a ^{2}F greater than ~ 0.001, corresponding to biosynthesis turnover time shorter than length of the incubation. The mean $^{2}F_{biomass}$ was ~ 1000 × natural abundance ($^{2}F_{nat}$ ~ 0.00015). The paired 15R3 coal amended with methylamine and hydrogen was ~ 200 × natural abundance. Methanol amendment had the second highest activity in 15R3 coal incubations, and the highest activity in the mixed lithology incubations. Mixed lithology amended with methanol and hydrogen + ammonium had the lowest activity, ~ 10 × natural abundance. The same relative activity between incubations remains without the Poisson error filter that was applied for cell ROIs in Figure 4 (see Supplemental Figure 4 with all ROIs). Some ROIs are above the 20 at. % D_2O label provided, but are considered within error of ≤ 20 at. % when accounting for the high label and long incubation variability. Kopf et al. (2015) showed that higher isotopic spikes and

← Figure 4: Violin plots displaying the kernel density distribution of (a) deuterium and (b) ^{15}N fractional isotope abundance from NanoSIMS ROIs that had D ion counts > 2 × shot noise. All cells are above natural abundance ^{2}F and ^{15}F, depicted as horizontal lines. 15R3 coal methylamine has a bimodal distribution in both ^{2}F and ^{15}F enrichment. The table includes number of ROIs in violin plots; the minimum, median, and maximum enrichment values for ^{2}F and turnover times in years for the range of ^{2}F values at three different water hydrogen assimilation constants (a_w); the minimum, median, and maximum enrichment values for ^{15}F and turnover times in years for the range of ^{15}F values. Methanol + hydrogen + ammonium had a ^{15}N isotope spike of 0.027 and methylamine samples had a ^{15}N isotope spike of 0.5. Gray shading differentiates 15R3 coal from mixed lithology samples.

longer cell retention times resulted in a larger spread of cellular anabolism values. For incubations with high levels of $^{2}H/^{1}H$ as used in this study, this amplifies the error in the conversion factor Kopf et al. calculated between bulk NanoSIMS and lipid-only deuterium (see Methods). Deuterium enrichment did not display a normal distribution across analyzed ROIs, but instead had a bimodal distribution as was also seen by Kopf et al. (2015). When comparing water assimilation within a chemostat monoculture grown with different turnover times (2 hrs versus 19 hrs), it was demonstrated that cells had higher water assimilation (~0.6 versus ~0.8) when turnover times were longer (Kopf 2015). Extending these findings to deep biosphere conditions, the longer turnover times based on the higher water assimilation constant-based (0.83) may be the most applicable to our system.

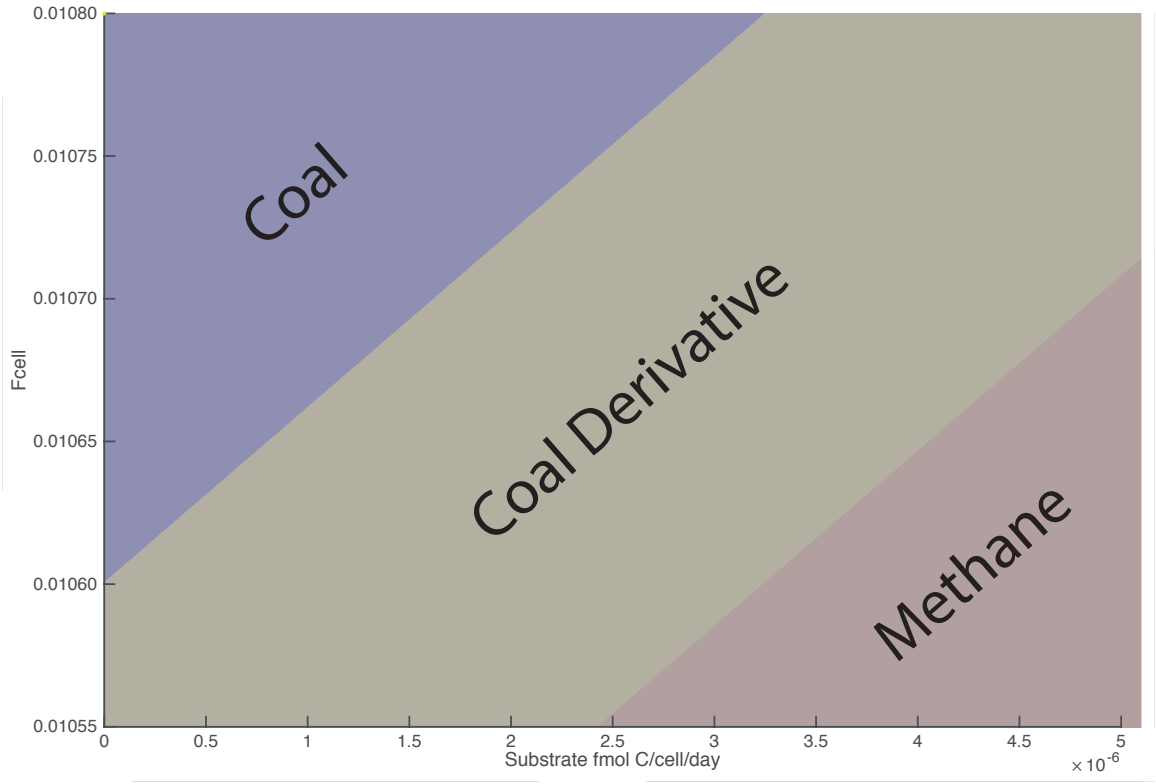

Figure 5: Carbon isotope mass balance to determine the range of substrate utilization rates (fmol C/cell/day) given the range of ^{13}C enrichment in cellular ROIs measured on the NanoSIMS (^{13}F 0.01063 to 0.01076) and the a range of native organic carbon substrates available and their in situ isotopic compositions (Supplemental Table 1).

^{15}N biomass incorporation mirrors ^{2}H for 15R3 coal amended with methylamine, with the highest anabolic activity observed in incubations without hydrogen amendment ($^{15}F_{biomass}$ is ~ 10

× natural abundance; $^{15}F_{nat}$ ~ 0.003) and lower, but detectable, anabolism when hydrogen was added. No ^{15}N activity was detected in mixed lithology amendments with methylamine ($^{15}F_{biomass}$ ~ natural abundance), but activity was detected with methanol + hydrogen + ammonium. No ^{15}N incorporation was seen in any autoclaved samples above the background threshold of natural abundance ^{15}N. There were no ROIs with ^{15}N incorporation without corresponding ^{2}H incorporation.

Single-cell biosynthesis rate-based turnover times were calculated based on ^{2}H and ^{15}N cellular enrichment (see Methods), where turnover times longer than 2.45 years are longer than the length of the incubation. Cells in 15R3 coal amended with methylamine had median deuterium-based turnover times of less than one year, regardless of a_w (Figure 4). 15R3 coal amended with methylamine + hydrogen had longer median turnover times of 6 to 13 years. 15R3 coal amended with methanol had the longest 15R3 coal turnover times of 33 to 63 years. Mixed lithology amended with methanol had a much shorter medium turnover time of 2 to 4 years, and even when amended with hydrogen (14 to 28 years) was still shorter than 15R3 coal with methanol only.

Nitrogen-based turnover times were slower than deuterium-based estimates for the methylamine (median 26 years) and methylamine + hydrogen (median 2,020 years) conditions, and faster than deuterium-based for ammonium condition (<1 year). Average anabolic rates were 1.99×10^{-6}, 1.45×10^{-4}, and 2.43×10^{-3} fmol N/cell/day for 15R3 coal amended with methylamine + hydrogen, 15R3 coal amended with methylamine, and mixed lithology amended with methanol + hydrogen + ammonium, respectively (Figure 4).

Discussion

Coal composition and phylotypes

Despite cell abundances that were substantially lower than expected from global depth trends and sediment surface concentrations, single-cell SIP-NanoSIMS successfully detected an active microbial assemblage in two terrestrial coalbeds buried for millions of years. Stable isotope incubations with the 15R3 coal and mixed lithology samples represent two coal types and

compare different methods of incubation preparation (intact coal chips versus homogenized mixed sample), labeled carbon sources (methylamine versus methanol), and labeled nitrogen sources (methylamine versus ammonium). This matrix of conditions were all amended with a passive anabolic activity tracer (D_2O) and incubated at in situ temperature (45 ^{o}C).

The 15R (upper) and 24/25R (lower) coals had different depositional histories, petrographic properties (Gross et al. 2015), and bacterial communities (Inagaki et al. 2015). The upper coal seams were predominantly coniferous in origin and deposited in a paralic environment (coastal, with marine and freshwater influence). The lower coal seams were dominantly angiosperm in origin and deposited in a limnic environment (freshwater). The 15R coal was also a less thermally altered lignite (dominant maceral humotelinite), whereas all other coal seams were in the transition between lignite and sub-bituminous coal (dominant maceral humodetrinite; Gross et al. 2015). Comparing the 16S rRNA gene phylogenic diversity of the 15R coal and 24/25R coalbeds, the shallower 15R coal had a higher relative abundance of Bacillales, whereas Gemmatimondales and Acidobacteria dominated the deeper coalbed. These coal samples, and the 16S rRNA genes recovered from the terrestrial samples as a whole, were dominated by heterotrophic bacteria. Heterotrophic bacteria, while able decompose coal to methyl-substrates, are not known to utilize methyl-substrates for catabolism under anaerobic conditions, such as this deeply buried coalbed. Anaerobic methyl metabolism is only known to archaea, which were not a significant proportion of the recovered 16S rRNA gene diversity. There was one archaeal 16S rRNA gene amplicon from a sample near the 25R coalbed related to *Methanosarcina* and sequences related to *Methanobacterium* were identified in methanogenic enrichments from 15R coal (Inagaki et al. 2015). Geochemical and biomarker evidence also points to an active methanogenic microbial coalbed community (Inagaki et al. 2015) that could be capable of our target methyl-metabolisms.

Carbon catabolism and anabolism

15R3 coal carbon catabolic rates ranged from 10^{-2} to 10^{-3} fmol C/cell/day from the provided ^{13}C-methyl-substrate, depending on which natural carbon source (methane, coal derivative, or coal) was mixed with the substrate. Comparing our carbon catabolic rates with those estimated from ^{35}S sulfate reduction (Hoehler & Jorgensen 2013), 15R3 coal incubation carbon catabolic rates

are between the lower end of marine surface sediment and higher end of deep subsurface marine sediment rates, and mixed lithology incubation carbon catabolism rates were closer to pure cultures. This difference between coal and mixed lithology incubations could be due to higher accessibility of fresh surfaces in the macerated mixed sample, relative to the intact pieces in 15R3 coal incubations, and/or a wider range of non-carbon substrates (e.g. iron minerals in sandstones and shales) from the mixing of multiple lithologies. Using NanoSIMS single-cell carbon enrichment and isotopic mass balance calculations, carbon anabolism (~ 10^{-6} fmol C/cell/day from substrate) was much lower than catabolism, and lower than any previously published deep biosphere anabolic rates. This is consistent with theories that deep biosphere cells have minimal, maintenance-only turnover of cellular biomass for energy conservation (Jørgensen & Marshall 2016), potentially aided by biomolecule recycling (Takano et al. 2010).

Considering the high percentage of label added (50 at. %), the DIC, CH_4, and single-cell NanoSIMS data indicate the methyl substrates added to the incubation were not the predominant carbon sources used to build the cellular biomass detected by ^{2}H and ^{15}N enrichment in our incubations. Instead, single-cell NanoSIMS and bulk geochemistry results suggest use of indigenous organic carbon substrates as opposed to in situ methane (-60 ‰) or DIC (-10 to 5 ‰). These findings are consistent with results from ODP Leg 201 Peru Margin where single-cell natural abundance carbon isotope measurements indicated a predominantly fossil organic carbon source (Biddle et al. 2008). However, NanoSIMS ^{13}C biomass measurements (-38 ‰) are about 15 ‰ more depleted than the coal (-25 ‰). One possibly is that microbes are accessing more depleted coal derivatives, such as the methoxyl group in vanillin. In NMR analysis of vanillin derived from microbial fermentation of lignin, the methoxyl group was 10 ‰ more depleted than the bulk vanillin molecule (Tenailleau et al. 2004). Alternatively, pressure dependent stable isotope fractionations have been observed for bulk biomass and fatty acids in heterotrophic bacteria (ΔδFA-glucose 15-18‰; Fang et al. 2006) that could allow for coalbed cells to be utilizing organic carbon sources with coal-carbon isotopic abundance (-25 ‰) while producing biomass that is -38 ‰, as seen here. While our incubations were not maintained at the in situ pressures that would produce these effects, there was little evidence of carbon anabolism from labeled substrates or significant carbon metabolic rates from any substrates, that would have significant altered the biomass in our incubations from its in situ composition. Therefore the

NanoSIMS is likely measuring the isotopic enrichment that would have been produced in situ and could explain the coal-biomass offset observed here.

Non-methyl carbon heterotrophy is further supported by results from the JAMSTEC incubations with a wider range of multi-carbon substrates. Out of all 15R3 incubations prepared onboard, ^{13}C-glucose had the highest enrichment in ^{13}C-DIC (~ 1,000 ‰; data not shown). Incubations with more coalbed relevant heterotrophic substrates, such as lignin monomer acids, also had labeled DIC production (~ 800 ‰ p-Coumaric acid ^{13}C (1, 2, 3); ~ 200 ‰ ferulic acid ^{13}C (1, 2, 3); data not shown) that was significantly higher than our methyl substrates (20 ‰; Table 1). This suggests heterotrophic coal degradation to methanogenesis substrates may occur at a faster rate than methylotrophic methanogenesis in this system. High in situ hydrogen concentrations (1 to 500 μM) indicate hydrogenotrophic methanogenesis is also operating far below the thermodynamic maximum (Inagaki et al. 2015), and multi-carbon organic substrates are more likely what supports deep life in the Shimokita coalbeds.

Hydrogen biosynthesis

Based on background 15R cell abundances of ~ 5 cells/cm^3 (~ 1920 mbsf), and similarly low cell abundances in samples that had no other signs of microbial activity, microorganisms in the 15R3 coal amended with methylamine had some growth during the 894 day incubation period (final cell concentration of 1920 cells/cm^3). This increase in cell abundance is supported by NanoSIMS data showing the cellular enrichment in both ^{2}H/^{1}H and ^{15}N/^{14}N, and the greatest number of isotopically enriched cells (Figure 4). Estimates from final incubation cell counts and NanoSIMS average cellular ^{2}F both independently calculated biosynthesis rate-based turnover times of less than one year for this incubation. 15R3 amended with methylamine also had a contiguous biomass doublet in NanoSIMS ^{1}H, ^{14}N, and ^{12}C ion counts (2 Coal; Figure 3), where only half of the sample had enrichment in ^{2}H (4.4 at. %) and ^{15}N (3.5 at. %) suggesting biomass existing prior to isotopic label exposure produced additional biomass after onset of incubation. This could be evidence of a dividing or sporulating cell. While most ROIs were active in this incubation, only about half of the cells were fully labeled (^{2}F 0.2). This could be the result of a microbial assemblage split into two modes, one that is more active and dividing and another that is undergoing maintenance-only biosynthesis. Kopf et al. (2015) also saw label uptake

heterogeneity became more pronounced as generation time increased (slower rates of growth), even in a monoculture chemostat. Therefore, this interesting physiological phenomenon does not appear limited to deep biosphere environments and does not require substrate partitioning (i.e. autotrophic versus heterotrophic populations) to occur, and should be explored further in both laboratory and environmental conditions.

Hydrogen inhibition

In cases where samples could be compared with and without hydrogen, hydrogen addition appeared to depress both ^{2}H and ^{15}N biosynthesis. Since hydrogen is generally produced by fermenters and removed by methanogens in coalbed methane systems (Strąpoć et al. 2011), it is likely the fermentive microbes that are inhibited by the addition of hydrogen if it is not kept under thermodynamic control by methanogens. Given that the hydrogen in our incubations should also be labeled from hydrogen exchange with deuterated water (Campbell et al. 2009), hydrogen derived methane produced in our system should have detectable $\delta D\text{-}CH_4$. The $\delta D\text{-}CH_4$ in 15R3 coal incubations did not indicate production via labeled hydrogen, and suggests hydrogenotrophic methanogens were not removing hydrogen from the incubations. Since we see little evidence of hydrogenotrophic methanogenesis, or other metabolisms that could remove hydrogen, our incubation hydrogen concentrations could inhibit fermenters. These findings demonstrating hydrogen as an inhibitor in our coalbed system are in contrast to the canonical idea that hydrogen is an important energy source for the deep biosphere (Adhikari et al. 2016; Pedersen 2000).

Nitrogen biosynthesis

There appeared to be a distinction in the nitrogen metabolism between the two sample types, 15R3 coal and mixed lithology. Biosynthesis turnover times based on 15R3 coal amended with ^{15}N-methylamine ranged from 19 to 40 years (Figure 4). While ^{2}F and ^{15}F were both highest in 15R3 coal amended with methylamine, N-based turnover times were fastest with ammonium amended incubations from mixed lithology (methanol + hydrogen + ammonium incubations; <1 to 3 years). This is due to turnover time calculations accounting for label dilution from background ammonium concentrations, and demonstrates the highest absolute rate ^{15}N assimilation was with ammonium. Surprisingly, no anabolism of ^{15}N was detected in 15R3 coal

incubations amended with ^{13}C-methanol, hydrogen, and ^{15}N-ammonium or mixed lithology samples amended with ^{15}N-methylamine ± hydrogen (Figure 4). Methylated amine concentrations are higher in estuarine environments than freshwater, and appear to sorb to the sediment fraction more than the aqueous fraction (Zhuang 2014). While unlikely that methylamine would survive deposition for millions of years in the coal, it is possible that a community buried under conditions where it was available might contain a microbial assemblage more predisposed to its utilization when provided as a substrate in our incubations. *Bacillus* sp. have also been shown to use methylamine as their sole nitrogen source (Bicknell & Owens 1980). Their higher relative abundance in 15R core 16S rRNA diversity screens is consistent with these nitrogen assimilation results suggesting fermentive bacteria may be anabolizing the nitrogen from methylamine in 15R3 coal incubations.

N versus C biosynthesis

NanoSIMS-based carbon anabolism rates were estimated to be ~10^{-6} fmol C/cell/day for the range of potential organic carbon sources used with the labeled substrate provided, across the full range of cellular ROI carbon isotope values from all incubations. 15R3 ^{15}N-methylamine nitrogen anabolism rates differed by two orders of magnitude for with and without hydrogen (10^{-6} fmol N/cell/day and 10^{-4} fmol N/cell/day, respectively), where the + hydrogen condition had the same anabolism rate as the carbon-based estimate for all incubations (10^{-6}). Methylamine utilization as a sole nitrogen source has been shown to be widespread among non-methylotrophic and non-methanogenic bacteria, even under anaerobic conditions, with apparent disregard of the carbon moiety of the molecule (Bicknell & Owens 1980). This suggests that only one population (i.e. methylotrophs) may be assimilating methylamine-derived carbon, but multiple community members may be capable of utilizing the nitrogen from methylamine (i.e. fermenters and methylotrophs). These results are consistent with hydrogen amendment not affecting the methylotrophic methanogen population present in both methylamine-amended 15R3 coal incubations, but hindering the dominant fermenting population utilizing methylamine for nitrogen but not carbon. Estimated DIC production rates from methylamine (catabolism) are all higher than nitrogen assimilation rates, such that the ^{13}C-labeled methyl group that was not anabolized from methylamine could have been catabolized and transferred to the DIC pool.

Mixed lithology amended with methanol + hydrogen + ammonium had the highest average nitrogen assimilation rate (2.43×10^{-3} fmol N/cell/day from ammonium). This ^{15}N-ammonium assimilation rate is 13-20% of the single-cell rates reported from NanoSIMS analysis of ^{13}C-bicarbonate and ^{13}C-acetate amendments with ^{15}N-ammonium from shallower (219 mbsf) sediment at this site (Morono et al. 2011). However, our carbon anabolic rates (~ 10^{-6} fmol C/cell/day) differ by three orders of magnitude from our ammonium assimilation rates, and four orders of magnitude from Morono et al. (~ 10^{-2} fmol C/cell/day). These discrepancies could be explained methodologically since the Morono et al. (2011) incubation amendments were different substrates and provided at higher concentrations, or could be a function of the difference in microbial community 2 km deeper into the Shimokita coalbed system. Despite the absolute rate differences, our findings are in agreement with Morono et al. (2011) that nitrogen, in the form of ammonium, is assimilated at a much higher rate than carbon in deep biosphere systems.

Conclusion

We provide the first deep biosphere application of a universal, passive tracer with extremely high sensitivity (D_2O) and single-cell resolution (NanoSIMS), as compared to previous methods based on bulk projections of sulfate reduction (D'Hondt et al. 2002; Parkes et al. 1990), single-cell natural abundance carbon (Biddle et al. 2006), or D:L racemization (Lomstein et al. 2012). SIP-NanoSIMS-based rates (months to years) appear much faster than these other methods (thousands of years), which may point to the necessity of single-cell techniques to determine accurate rates in low activity systems. Despite extremely low cell abundances, our incubations with deeply buried terrestrial coal and associated lithologies were successful in determining average deuterium-based turnover times ranging from less than a year to 63 years after an extended incubation time of 2.5 years at in situ temperatures. The bimodal distribution of single-cell deuterium enrichment for the most active incubation (15R3 coal amended with methylamine) supports the idea of a deep coalbed microbial assemblage that is capable of activation and growth when resources become available, while simultaneously sustaining a community dominated by maintenance over growth. We find that nitrogen was assimilated from both methylamine and ammonium, and the pattern of methylamine utilization was consistent

with the coal depositional setting and microbial phylotypes. We also support previous findings that nitrogen from ammonium is assimilated more readily than carbon in deep biosphere SIP-NanoSIMS incubations and that most deep biosphere cells appear to be viable (Morono et al. 2011). Methyl-substrate specific carbon anabolic rates were much slower than any previously published carbon rates (~ 10^{-6} fmol C/cell/day) where the main carbon source anabolized appeared to be in situ fossil organic carbon, as has been seen by others (Biddle et al. 2006), in a system where bacterial coal degradation may dominate archaeal methanogenesis.

References

Adhikari RR, Glombitza C, Nickel JC, Anderson CH, Dunlea AG, Spivack AJ, Murray RW, D'Hondt S, and Kallmeyer J. 2016. Hydrogen utilization potential in subsurface sediments. *Frontiers in Microbiology* 7. 10.3389/fmicb.2016.00008

Auguie B. 2012. gridExtra: functions in Grid graphics. R package version 0.9.1 ed.

Berry D, Mader E, Lee TK, Woebken D, Wang Y, Zhu D, Palatinszky M, Schintlmeister A, Schmid MC, Hanson BT, Shterzer N, Mizrahi I, Rauch I, Decker T, Bocklitz T, Popp Jr, Gibson CM, Fowler PW, Huang WE, and Wagner M. 2015. Tracking heavy water (D2O) incorporation for identifying and sorting active microbial cells. *Proceedings of the National Academy of Sciences* 112:E194-E203. 10.1073/pnas.1420406112

Bicknell B, and Owens J. 1980. Utilization of methyl amines as nitrogen sources by non-methylotrophs. *Microbiology* 117:89-96.

Biddle JF, Fitz-Gibbon S, Schuster SC, Brenchley JE, and House CH. 2008. Metagenomic signatures of the Peru Margin subseafloor biosphere show a genetically distinct environment. *Proceedings of the National Academy of Sciences* 105:10583-10588. 10.1073/pnas.0709942105

Biddle JF, Lipp JS, Lever MA, Lloyd KG, S√ ∏rensen KB, Anderson R, Fredricks HF, Elvert M, Kelly TJ, Schrag DP, Sogin ML, Brenchley JE, Teske A, House CH, and Hinrichs K-U. 2006. Heterotrophic Archaea dominate sedimentary subsurface ecosystems off Peru. *Proceedings of the National Academy of Sciences of the United States of America* 103:3846-3851. 10.1073/pnas.0600035103

Biddle JF, Sylvan JB, Brazelton WJ, Tully BJ, Edwards KJ, Moyer CL, Heidelberg JF, and Nelson WC. 2011. Prospects for the Study of Evolution in the Deep Biosphere. *Frontiers in Microbiology* 2:285. 10.3389/fmicb.2011.00285

Campbell BJ, Li C, Sessions AL, and Valentine DL. 2009. Hydrogen isotopic fractionation in lipid biosynthesis by H2-consuming Desulfobacterium autotrophicum. *Geochimica et Cosmochimica Acta* 73:2744-2757. http://dx.doi.org/10.1016/j.gca.2009.02.034

Ciobanu M-C, Burgaud G, Dufresne A, Breuker A, Redou V, Ben Maamar S, Gaboyer F, Vandenabeele-Trambouze O, Lipp JS, Schippers A, Vandenkoornhuyse P, Barbier G, Jebbar M, Godfroy A, and Alain K. 2014. Microorganisms persist at record depths in the subseafloor of the Canterbury Basin. *ISME J* 8:1370-1380. 10.1038/ismej.2013.250

Coplen TB, Brand WA, Gehre M, Gröning M, Meijer HAJ, Toman B, and Verkouteren RM. 2006. New Guidelines for δ13C Measurements. *Analytical Chemistry* 78:2439-2441. 10.1021/ac052027c

D'Hondt S, Inagaki F, Zarikian CA, Abrams LJ, Dubois N, Engelhardt T, Evans H, Ferdelman T, Gribsholt B, Harris RN, Hoppie BW, Hyun J-H, Kallmeyer J, Kim J, Lynch JE, McKinley CC, Mitsunobu S, Morono Y, Murray RW, Pockalny R, Sauvage J, Shimono T, Shiraishi F, Smith DC, Smith-Duque CE, Spivack AJ, Steinsbu BO, Suzuki Y, Szpak M, Toffin L, Uramoto G, Yamaguchi YT, Zhang G-l, Zhang X-H, and Ziebis W. 2015. Presence of oxygen and aerobic communities from sea floor to basement in deep-sea sediments. *Nature Geosci* 8:299-304. 10.1038/ngeo2387

D'Hondt S, Jørgensen BB, Miller DJ, Batzke A, Blake R, Cragg BA, Cypionka H, Dickens GR, Ferdelman T, Hinrichs K-U, Holm NG, Mitterer R, Spivack A, Wang G, Bekins B, Engelen B, Ford K, Gettemy G, Rutherford SD, Sass H, Skilbeck CG, Aiello IW, Guèrin G, House CH, Inagaki F, Meister P, Naehr T, Niitsuma S, Parkes RJ, Schippers A, Smith DC, Teske A, Wiegel J, Padilla CN, and Acosta JLS. 2004. Distributions of Microbial Activities in Deep Subseafloor Sediments. *Science* 306:2216-2221. 10.1126/science.1101155

D'Hondt S, Rutherford S, and Spivack AJ. 2002. Metabolic Activity of Subsurface Life in Deep-Sea Sediments. *Science* 295:2067-2070. 10.1126/science.1064878

Eichorst SA, Strasser F, Woyke T, Schintlmeister A, Wagner M, and Woebken D. 2015. Advancements in the application of NanoSIMS and Raman microspectroscopy to investigate the activity of microbial cells in soils. *FEMS Microbiology Ecology* 91. 10.1093/femsec/fiv106

Expedition 337 Scientists. 2013. Methods. *Proceedings of IODP* 337. 10.2204/iodp.proc.337.102.2013

Fang J, Uhle M, Billmark K, Bartlett DH, and Kato C. 2006. Fractionation of carbon isotopes in biosynthesis of fatty acids by a piezophilic bacterium Moritella japonica strain DSK1. *Geochimica et Cosmochimica Acta* 70:1753-1760. http://dx.doi.org/10.1016/j.gca.2005.12.011

Fry JC, Horsfield B, Sykes R, Cragg BA, Heywood C, Kim GT, Mangelsdorf K, Mildenhall DC, Rinna J, Vieth A, Zink K-G, Sass H, Weightman AJ, and Parkes RJ. 2009. Prokaryotic Populations and Activities in an Interbedded Coal Deposit, Including a Previously Deeply Buried Section (1.6,Äì2.3 km) Above ‚àº 150 Ma Basement Rock. *Geomicrobiology Journal* 26:163-178. 10.1080/01490450902724832

Gross D, Bechtel A, and Harrington GJ. 2015. Variability in coal facies as reflected by organic petrological and geochemical data in Cenozoic coal beds offshore Shimokita (Japan) - IODP Exp. 337. *International Journal of Coal Geology* 152, Part B:63-79. http://dx.doi.org/10.1016/j.coal.2015.10.007

Hayes JM. 2004. An introduction to isotopic calculations. *Woods Hole Oceanographic Institution, Woods Hole, MA* 2543.

Hoehler TM, and Jorgensen BB. 2013. Microbial life under extreme energy limitation. *Nat Rev Micro* 11:83-94.

Horsfield B, Schenk HJ, Zink K, Ondrak R, Dieckmann V, Kallmeyer J, Mangelsdorf K, di Primio R, Wilkes H, Parkes RJ, Fry J, and Cragg B. 2006. Living microbial ecosystems within the active zone of catagenesis: Implications for feeding the deep biosphere. *Earth and Planetary Science Letters* 246:55-69. http://dx.doi.org/10.1016/j.epsl.2006.03.040

Inagaki F, Hinrichs K-U, Kubo Y, Bowles MW, Heuer VB, Hong W-L, Hoshino T, Ijiri A, Imachi H, Ito M, Kaneko M, Lever MA, Lin Y-S, Methé BA, Morita S, Morono Y, Tanikawa W, Bihan M, Bowden SA, Elvert M, Glombitza C, Gross D, Harrington GJ, Hori T, Li K, Limmer D, Liu C-H, Murayama M, Ohkouchi N, Ono S, Park Y-S, Phillips SC, Prieto-Mollar X, Purkey M, Riedinger N, Sanada Y, Sauvage J, Snyder G, Susilawati R, Takano Y, Tasumi E, Terada T, Tomaru H, Trembath-Reichert E, Wang DT, and Yamada Y. 2015. Exploring deep microbial life in coal-bearing sediment down to ~2.5 km below the ocean floor. *Science* 349:420-424. 10.1126/science.aaa6882

Inagaki F, Hinrichs K-U, and Kubo Ys. 2010. *Integrated Ocean Drilling Program Expedition 337 Scientific Prospectus*: Integrated Ocean Drilling Program Management International, Inc.

Inagaki F, Hinrichs K-U, Kubo Ys, and Scientists E. 2012. *Deep coalbed biosphere off Shimokita*: Integrated Ocean Drilling Program Management International, Inc.

Jørgensen BB, and Marshall IPG. 2016. Slow Microbial Life in the Seabed. *Annual Review of Marine Science* 8:311-332. doi:10.1146/annurev-marine-010814-015535

Kallmeyer J, Pockalny R, Adhikari RR, Smith DC, and D,ÄôHondt S. 2012. Global distribution of microbial abundance and biomass in subseafloor sediment. *Proceedings of the National Academy of Sciences* 109:16213-16216. 10.1073/pnas.1203849109

Kellermann MY, Yoshinaga MY, Wegener G, Krukenberg V, and Hinrichs K-U. 2016. Tracing the production and fate of individual archaeal intact polar lipids using stable isotope probing. *Organic Geochemistry* 95:13-20. http://dx.doi.org/10.1016/j.orggeochem.2016.02.004

Kikuchi S, Makita H, Konno U, Shiraishi F, Ijiri A, Takai K, Maeda M, and Takahashi Y. 2016. Limited reduction of ferrihydrite encrusted by goethite in freshwater sediment. *Geobiology*:n/a-n/a. 10.1111/gbi.12181

Konyukhov AI. 2010. Continental margins as global oil and gas accumulation belts: The West Pacific belt. *Lithology and Mineral Resources* 45:465-485. 10.1134/s0024490210050056

Kopf SH. 2015. From lakes to lungs: assessing microbial activity in diverse environments Doctor of Philosophy. California Institute of Technology.

Kopf SH, McGlynn SE, Green-Saxena A, Guan Y, Newman DK, and Orphan VJ. 2015. Heavy water and 15N labelling with NanoSIMS analysis reveals growth rate-dependent metabolic heterogeneity in chemostats. *Environmental Microbiology* 17:2542-2556. 10.1111/1462-2920.12752

Kopf SH, Sessions AL, Cowley ES, Reyes C, Van Sambeek L, Hu Y, Orphan VJ, Kato R, and Newman DK. 2016. Trace incorporation of heavy water reveals slow and heterogeneous pathogen growth rates in cystic fibrosis sputum. *Proceedings of the National Academy of Sciences* 113:E110-E116. 10.1073/pnas.1512057112

Leloup J, Fossing H, Kohls K, Holmkvist L, Borowski C, and Jørgensen BB. 2009. Sulfate-reducing bacteria in marine sediment (Aarhus Bay, Denmark): abundance and diversity related to geochemical zonation. *Environmental Microbiology* 11:1278-1291. 10.1111/j.1462-2920.2008.01855.x

Lipp JS, Morono Y, Inagaki F, and Hinrichs K-U. 2008. Significant contribution of Archaea to extant biomass in marine subsurface sediments. *Nature* 454:991-994. http://www.nature.com/nature/journal/v454/n7207/suppinfo/nature07174_S1.html

Lomstein BA, Langerhuus AT, D'Hondt S, Jorgensen BB, and Spivack AJ. 2012. Endospore abundance, microbial growth and necromass turnover in deep sub-seafloor sediment. *Nature* 484:101-104.

Morono Y, Terada T, Kallmeyer J, and Inagaki F. 2013. An improved cell separation technique for marine subsurface sediments: applications for high-throughput analysis using flow cytometry and cell sorting. *Environmental Microbiology* 15:2841-2849. 10.1111/1462-2920.12153

Morono Y, Terada T, Nishizawa M, Ito M, Hillion F, Takahata N, Sano Y, and Inagaki F. 2011. Carbon and nitrogen assimilation in deep subseafloor microbial cells. *Proceedings of the National Academy of Sciences* 108:18295-18300. 10.1073/pnas.1107763108

Morono Y, Terada T, Yamamoto Y, Xiao N, Hirose T, Sugeno M, Ohwada N, and Inagaki F. 2015. Intact preservation of environmental samples by freezing under an alternating magnetic field. *Environmental Microbiology Reports* 7:243-251. 10.1111/1758-2229.12238

Neuwirth E. 2014. RColorBrewer. R package version 1.1-2 ed.

Parkes RJ, Cragg B, Roussel E, Webster G, Weightman A, and Sass H. 2014. A review of prokaryotic populations and processes in sub-seafloor sediments, including biosphere:geosphere interactions. *Marine Geology* 352:409-425. http://dx.doi.org/10.1016/j.margeo.2014.02.009

Parkes RJ, Cragg BA, Fry JC, Herbert RA, Wimpenny JWT, Allen JA, and Whitfield M. 1990. Bacterial Biomass and Activity in Deep Sediment Layers from the Peru Margin [and Discussion]. *Philosophical Transactions of the Royal Society of London A: Mathematical, Physical and Engineering Sciences* 331:139-153. 10.1098/rsta.1990.0061

Parkes RJ, Wellsbury P, Mather ID, Cobb SJ, Cragg BA, Hornibrook ERC, and Horsfield B. 2007. Temperature activation of organic matter and minerals during burial has the potential to

sustain the deep biosphere over geological timescales. *Organic Geochemistry* 38:845-852. http://dx.doi.org/10.1016/j.orggeochem.2006.12.011

Pedersen K. 2000. Exploration of deep intraterrestrial microbial life: current perspectives. *FEMS Microbiology Letters* 185:9-16. 10.1111/j.1574-6968.2000.tb09033.x

Polerecky L, Adam B, Milucka J, Musat N, Vagner T, and Kuypers MMM. 2012. Look@NanoSIMS – a tool for the analysis of nanoSIMS data in environmental microbiology. *Environmental Microbiology* 14:1009-1023. 10.1111/j.1462-2920.2011.02681.x

Postgate JR, and Hunter JR. 1963. Acceleration of Bacterial Death by Growth Substrates. *Nature* 198:273-273.

R Core Team. 2015. R: A Language and Environment for Statistical Computing. Vienna, Austria: R Foundation for Statistical Computing.

Rebata-Landa V, and Santamarina JC. 2006. Mechanical limits to microbial activity in deep sediments. *Geochemistry, Geophysics, Geosystems* 7:n/a-n/a. 10.1029/2006GC001355

Strąpoć D, Mastalerz M, Dawson K, Macalady J, Callaghan AV, Wawrik B, Turich C, and Ashby M. 2011. Biogeochemistry of microbial coal-bed methane.

Takano Y, Chikaraishi Y, Ogawa NO, Nomaki H, Morono Y, Inagaki F, Kitazato H, Hinrichs K-U, and Ohkouchi N. 2010. Sedimentary membrane lipids recycled by deep-sea benthic archaea. *Nature Geosci* 3:858-861.

Tenailleau EJ, Lancelin P, Robins RJ, and Akoka S. 2004. Authentication of the origin of vanillin using quantitative natural abundance 13C NMR. *Journal of agricultural and food chemistry* 52:7782-7787.

Toki T, Higa R, Ijiri A, Tsunogai U, and Ashi J. 2014. Origin and transport of pore fluids in the Nankai accretionary prism inferred from chemical and isotopic compositions of pore water at cold seep sites off Kumano. *Earth, Planets and Space* 66:1-14.

Torres ME, Mix AC, and Rugh WD. 2005. Precise δ13C analysis of dissolved inorganic carbon in natural waters using automated headspace sampling and continuous-flow mass spectrometry. *Limnology and Oceanography: Methods* 3:349-360. 10.4319/lom.2005.3.349

Wegener G, Bausch M, Holler T, Thang NM, Prieto Mollar X, Kellermann MY, Hinrichs K-U, and Boetius A. 2012. Assessing sub-seafloor microbial activity by combined stable isotope probing with deuterated water and 13C-bicarbonate. *Environmental Microbiology* 14:1517-1527. 10.1111/j.1462-2920.2012.02739.x

Whitman WB, Coleman DC, and Wiebe WJ. 1998. Prokaryotes: The unseen majority. *Proceedings of the National Academy of Sciences* 95:6578-6583.

Wickham H. 2009. *ggplot2: elegant graphics for data analysis*: Springer, New York.

Wickham H, and Francois R. 2015. dplyr: A Grammar of Data Manipulation. R package version 0.4.1 ed.

Xie S, Lipp JS, Wegener G, Ferdelman TG, and Hinrichs K-U. 2013. Turnover of microbial lipids in the deep biosphere and growth of benthic archaeal populations. *Proceedings of the National Academy of Sciences* 110:6010-6014. 10.1073/pnas.1218569110

Zeng X, Birrien J-L, Fouquet Y, Cherkashov G, Jebbar M, Querellou J, Oger P, Cambon-Bonavita M-A, Xiao X, and Prieur D. 2009. Pyrococcus CH1, an obligate piezophilic hyperthermophile: extending the upper pressure-temperature limits for life. *ISME J* 3:873-876.

Zhang X, Gillespie AL, and Sessions AL. 2009. Large D/H variations in bacterial lipids reflect central metabolic pathways. *Proceedings of the National Academy of Sciences* 106:12580-12586. 10.1073/pnas.0903030106

Zhuang G. 2014. Methylotrophic methanogenesis and potential methylated substrates in marine sediment Doctoral. Universität Bremen.

Zilversmit DB, Entenman C, and Fishler MC. 1943. ON THE CALCULATION OF "TURNOVER TIME" AND "TURNOVER RATE" FROM EXPERIMENTS INVOLVING THE USE OF LABELING AGENTS. *The Journal of General Physiology* 26:325-331.

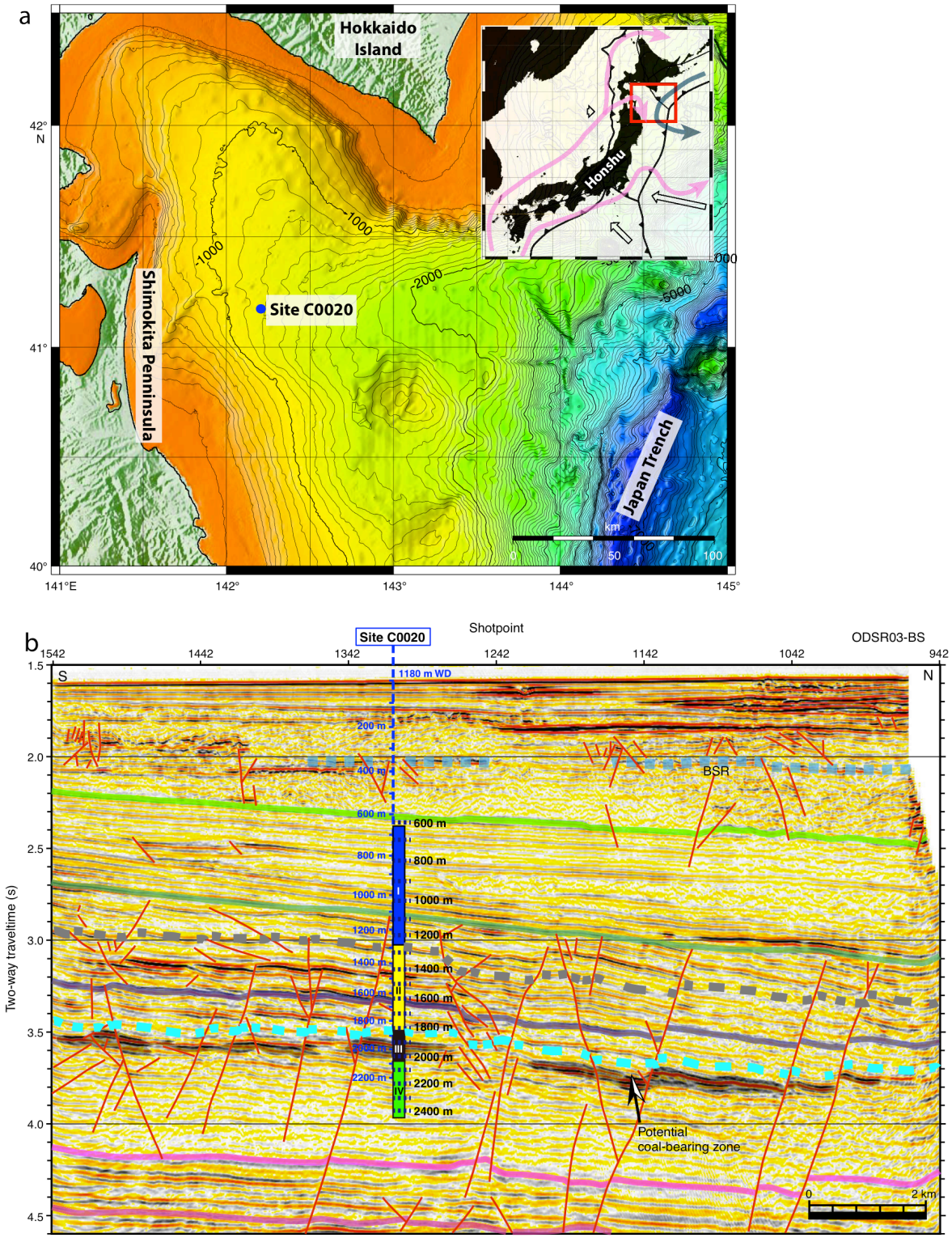

Supplemental Figure 1: a. Location of Site C0020 borehole off Shimokita Peninsula, Northern Honshu Island with bathymetry of the region. Inset contains plate configuration, dominant currents (Kuroshio and Tsushima) and bathymetric map location (red square). b. Seismic profile overlaid with IODP Expedition core recovery. Unit III and IV were used for incubations in this study. Dashed gray line indicates transition from offshore marine. Figures adapted from (2010).

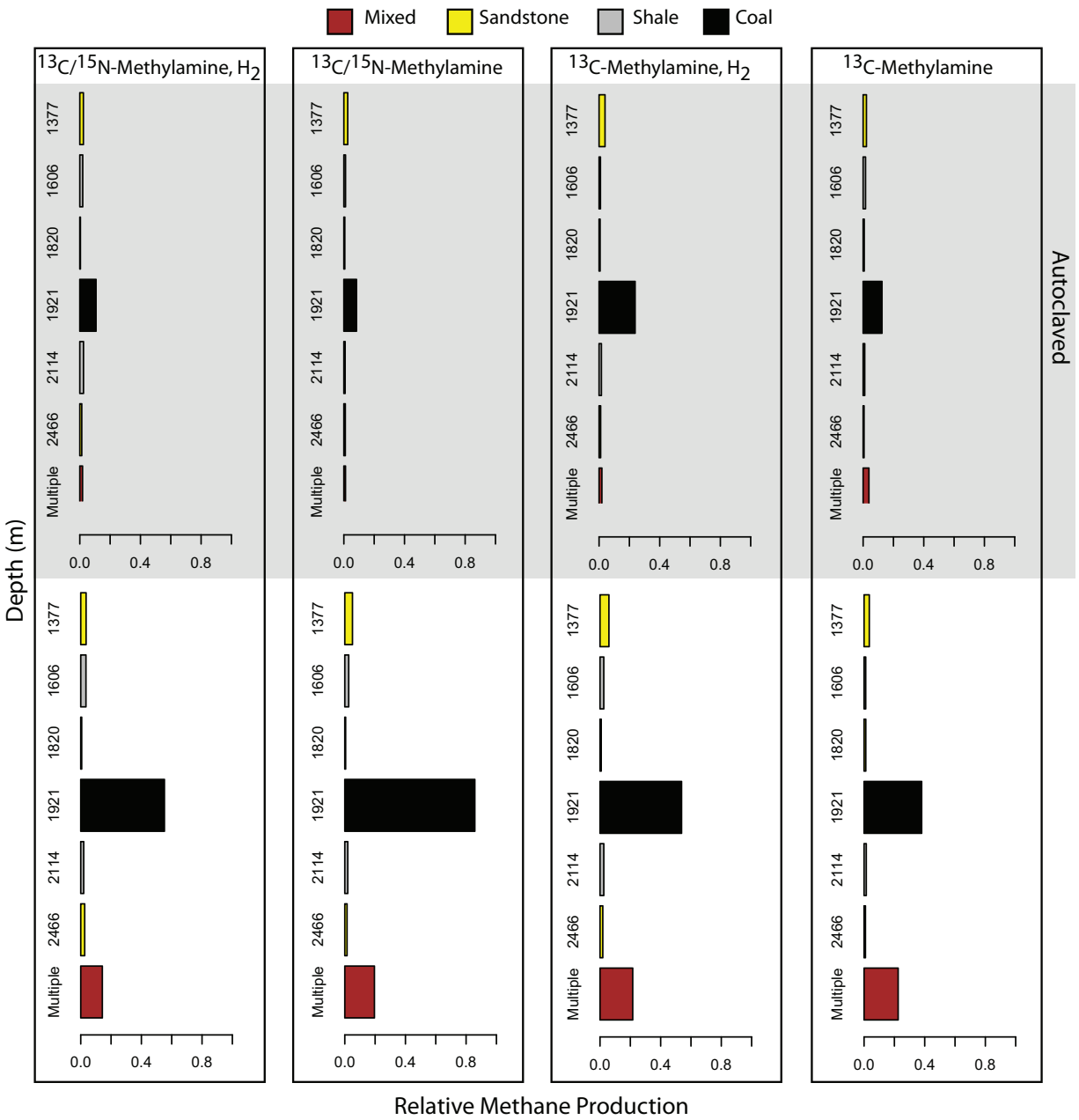

Supplemental Figure 2: Relative methane production from all methylamine and methanol incubations, by lithology.

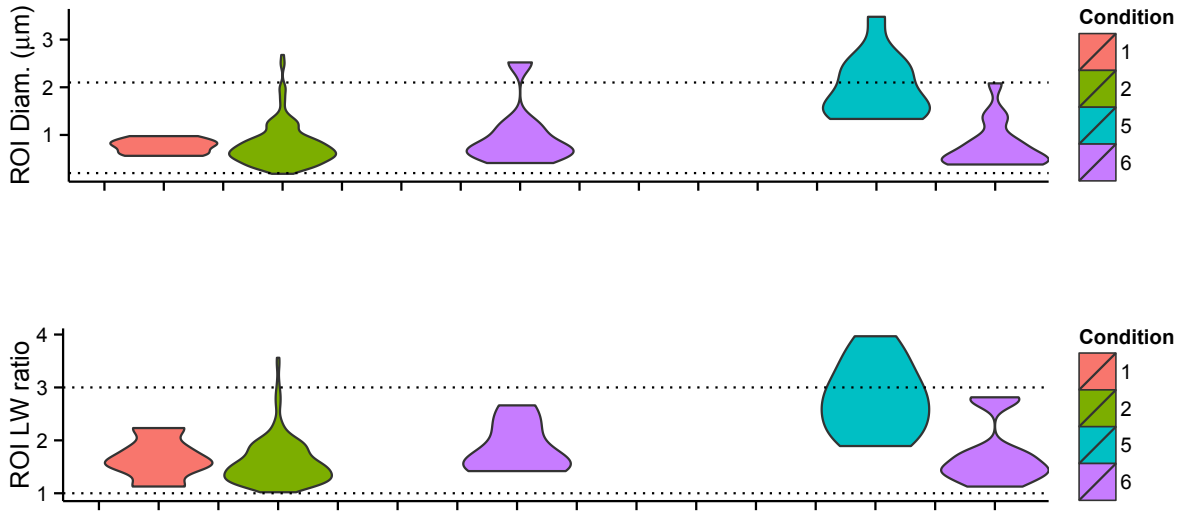

Supplemental Figure 3: Estimated maximal cell diameter (um) and length to width ratios calculated from NanoSIMS ROIs. Dashed lines indicate deep biosphere ranges (Kallmeyer et al. 2012). Conditions: 1 – methylamine + hydrogen, 2 – methylamine, 5 - methanol + hydrogen + ammonium, 6 – methanol. The first four samples are 15R3 coal and the last two are mixed lithology.

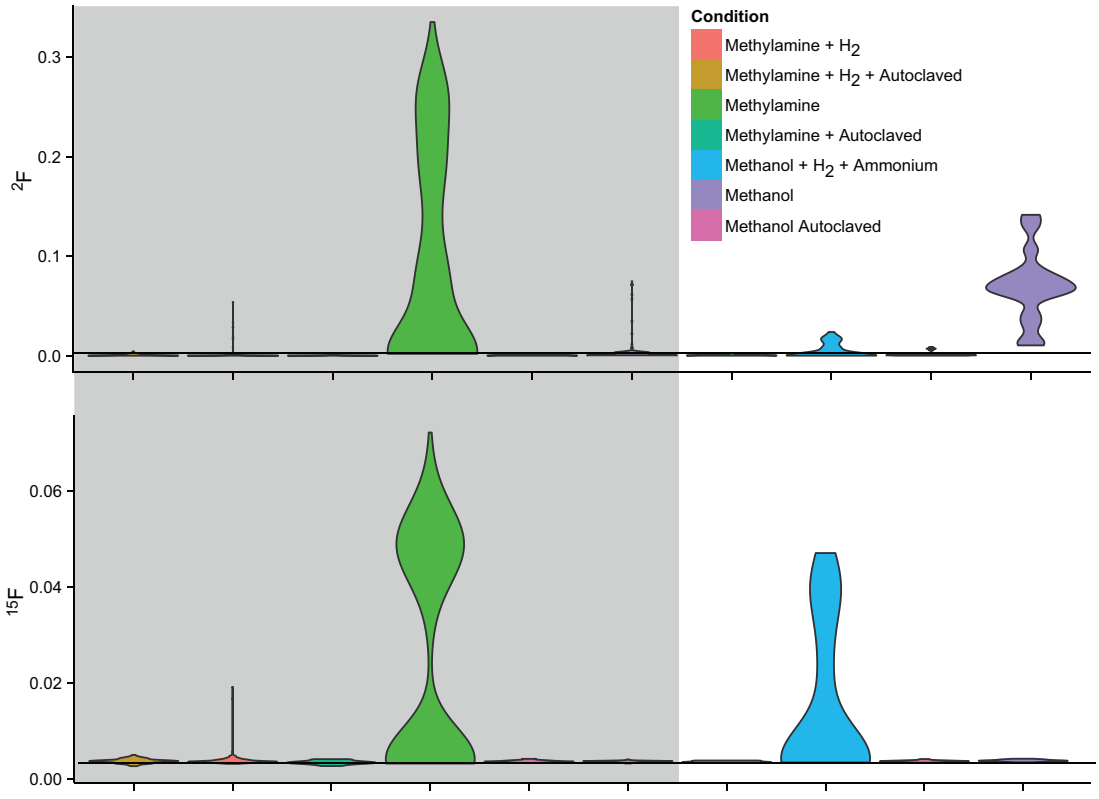

Supplemental Figure 4: Violin plots displaying the kernel density estimation of ^{2}H and ^{15}N fractional abundance from all NanoSIMS ROIs. Gray shading differentiates 15R3 coal (gray) and from mixed lithology samples. No ROIs were recovered from the autoclaved methanol + hydrogen + ammonium conditions so it is not included.

Supplemental Table 1: Isotopic ratios and fractional abundances used for reference and isotope mass balance calculations.

	R	F
^{2}H VSMOW	0.00015576	0.00015574
^{2}H Nat. Abd.	0.00011570	0.00011569
^{13}C VPDB	0.0112372	0.0111123
^{13}C Nat. Abd.	0.0110	0.0109
^{13}C 2km Coal	0.010979	0.010860
^{13}C 2km Methane	0.010563	0.010453
^{15}N Air	0.003677	0.003664
^{15}N Nat. Abd.	0.003642	0.003629
^{15}N 2km Coal	0.003703	0.003689

Supplemental Table 2: IODP Core Identification, top of core depth in meters below seafloor (mbsf), estimated in situ temperature calculated from borehole temperature gradient of 24.0^{o}C/km, porosity ranges, lithology from Site C0020 report. Raw and most likely cell abundances (cells/cm^{3}) and taxonomic information from 16S rRNA gene iTag sequencing from Inagaki et al. 2015.

IODP Core	Depth (mbsf)	Porosity (%)	Lithology	Most Likely (cells/cm^{3})	Dominant Order(s)	Unique Phyla
15R-2	1920.4	24-32	Coal/Shale	3.69	Bacillales	Verrucomicrobia, Tenericutes
15R-7	1925.8	24-32	Coal/Shale	4.66		
19R-1	1951.2	24-32	Siltstone/Shale	0.45	Lactobacillales, Micrococcales	Spirochaetes
19R-5	1954.5	24-32	Siltstone/Shale	30.54		
20R-3	1961.6	25-48	Sandy siltstone	0.10	Micrococcales, Clostridales	Planctomycetes
23R-8	1989.5	25-48	Sandstone	0.20	Gemmatimondales	Gemmatimondales
24R-3	1994.0	25-38	Coal/Shale	6.91	Gemmatimondales	
25R-3	1999.0	25-38	Coal/Sandstone	2.51	Granulicella, Clostridales	Acidobacteria